Toxoplasma gondii salvages sphingolipids from the host Golgi through the rerouting of selected Rab vesicles to the parasitophorous vacuole

Romano, Julia D ; Sonda, Sabrina ; Bergbower, Emily ; Smith, Maria Elisa ; Coppens, Isabelle

Abstract: The obligate intracellular protozoan Toxoplasma gondii actively invades mammalian cells and, upon entry, forms its own membrane-bound compartment, named the parasitophorous vacuole (PV). Within the PV, the parasite replicates and scavenges nutrients, including lipids, from host organelles. Although T. gondii can synthesize sphingolipids de novo, it also scavenges these lipids from the host Golgi. How the parasite obtains sphingolipids from the Golgi remains unclear, as the PV avoids fusion with host organelles. In this study, we explore the host Golgi-PV interaction and evaluate the importance of host-derived sphingolipids for parasite growth. We demonstrate that the PV preferentially localizes near the host Golgi early during infection and remains closely associated with this organelle throughout infection. The parasite subverts the structure of the host Golgi, resulting in its fragmentation into numerous ministacks, which surround the PV, and hijacks host Golgi-derived vesicles within the PV. These vesicles, marked with Rab14, Rab30, or Rab43, colocalize with host-derived sphingolipids in the vacuolar space. Scavenged sphingolipids contribute to parasite replication since alterations in host sphingolipid metabolism are detrimental for the parasite's growth. Thus our results reveal that T. gondii relies on host-derived sphingolipids for its development and scavenges these lipids via Golgi-derived vesicles.

DOI: https://doi.org/10.1091/mbc.E12-11-0827

Toxoplasma gondii salvages sphingolipids from the host Golgi through the rerouting of selected Rab vesicles to the parasitophorous vacuole

Julia D. Romano[a], Sabrina Sonda[b], Emily Bergbower[a], Maria Elisa Smith[a], and Isabelle Coppens[a]
[a]Department of Molecular Microbiology and Immunology, Johns Hopkins University Bloomberg School of Public Health, Baltimore, MD 21205; [b]Institute of Parasitology, University of Zurich, CH-8057 Zurich, Switzerland

ABSTRACT **The obligate intracellular protozoan *Toxoplasma gondii* actively invades mammalian cells and, upon entry, forms its own membrane-bound compartment, named the parasitophorous vacuole (PV). Within the PV, the parasite replicates and scavenges nutrients, including lipids, from host organelles. Although *T. gondii* can synthesize sphingolipids de novo, it also scavenges these lipids from the host Golgi. How the parasite obtains sphingolipids from the Golgi remains unclear, as the PV avoids fusion with host organelles. In this study, we explore the host Golgi–PV interaction and evaluate the importance of host-derived sphingolipids for parasite growth. We demonstrate that the PV preferentially localizes near the host Golgi early during infection and remains closely associated with this organelle throughout infection. The parasite subverts the structure of the host Golgi, resulting in its fragmentation into numerous ministacks, which surround the PV, and hijacks host Golgi–derived vesicles within the PV. These vesicles, marked with Rab14, Rab30, or Rab43, colocalize with host-derived sphingolipids in the vacuolar space. Scavenged sphingolipids contribute to parasite replication since alterations in host sphingolipid metabolism are detrimental for the parasite's growth. Thus our results reveal that *T. gondii* relies on host-derived sphingolipids for its development and scavenges these lipids via Golgi-derived vesicles.**

Monitoring Editor
Howard Riezman
University of Geneva

Received: Nov 21, 2012
Revised: Apr 10, 2013
Accepted: Apr 12, 2013

INTRODUCTION

The obligate intracellular protozoan *Toxoplasma gondii* is an opportunistic pathogen that is associated with congenital birth defects and severe ailments, such as encephalitis, in immunocompromised individuals. The host immune response restricts *T. gondii* replication, leading to the conversion of the parasite to its cyst form, which remains dormant in the brain and muscles (Luft and Remington, 1992).

On entry into a mammalian cell, *T. gondii* creates its own membrane-bound compartment, termed the parasitophorous vacuole (PV). This vacuole does not share any characteristics with a phagosome, as the process of invasion is entirely driven by the parasite and is distinct from phagocytosis (Morisaki *et al.*, 1995; Dobrowolski and Sibley, 1996; Suss-Toby *et al.*, 1996). A successful infection is dependent on the biogenesis and maturation of the PV into a replication-permissive niche, in a process mediated by the parasite. The PV membrane excludes most host plasma membrane transmembrane proteins during invasion and resists fusion with host organelles (Mordue *et al.*, 1999a; Charron and Sibley, 2004). Instead, the PV membrane is composed of many proteins secreted by the parasite (reviewed in Cesbron-Delauw *et al.*, 2008; Nam, 2009). Although the PV does not fuse with the host endolysosomal system (Mordue *et al.*, 1999b), it forms a tight association with host mitochondria and endoplasmic reticulum (ER; Sinai *et al.*, 1997). Additional transformations of the PV include the formation of pores across the PV membrane (Schwab *et al.*, 1994) and the development of a tubulovesicular network within the PV lumen (Nichols *et al.*, 1983; Sibley *et al.*, 1995). These unique parasite-induced modifications of the vacuole are hypothesized to be important for nutrient acquisition.

This article was published online ahead of print in MBoC in Press (http://www.molbiolcell.org/cgi/doi/10.1091/mbc.E12-11-0827) on April 24, 2013.

Address correspondence to: Isabelle Coppens (icoppens@jhsph.edu), Julia D. Romano (jromano@jhsph.edu).

Abbreviations used: MTOC, microtubule-organizing center; PDM, product of the differences from the mean; p.i., postinfection; PV, parasitophorous vacuole; PVM, PV membrane; TGN, *trans*-Golgi network.

Supplemental Material can be found at:
http://www.molbiolcell.org/content/suppl/2013/04/22/mbc.E12-11-0827v1.DC1.html

After invasion, the parasite migrates toward the perinuclear region of its host cell and localizes near the host microtubule-organizing center (MTOC) and the host Golgi (Coppens *et al.*, 2006; Romano *et al.*, 2008; Walker *et al.*, 2008). The Golgi–MTOC region resides at the intersection of the endocytic and exocytic pathways of the cell and is rich in endosomes, lysosomes, and post-Golgi vesicles. The positioning of the PV in this region of the cell may facilitate interception of host vesicular trafficking by *T. gondii* to satisfy the parasite's requirement for nutrients such as lipids. The parasite has a marked requirement for host lipids that are derived from lysosomes (e.g., cholesterol) or from the Golgi apparatus (e.g., ceramide; de Melo and De Souza, 1996; Bisanz *et al.*, 2006; Coppens, 2006). In the case of cholesterol, *T. gondii* contains large amounts of cholesterol, which it scavenges from plasma low-density lipoproteins (LDLs) via host endocytic compartments (Coppens *et al.*, 2000, 2006). The parasite sequesters nutrient-filled host lysosomes within invaginations of the PV membrane, thereby obtaining cholesterol from the host endocytic network (Coppens *et al.*, 2006). The cholesterol is then ultimately internalized by the parasite via ABCG transporters (Ehrenman *et al.*, 2010).

In eukaryotic cells, sphingolipids have an important role in cellular architecture, signaling, the cell cycle, and apoptosis (Breslow and Weissman, 2010). Sphingolipids are also ubiquitous membrane components in pathogenic protozoa and have been extensively studied in Trypanosomatids and the malaria parasite (reviewed in Zhang *et al.*, 2010). Our lipidomic analysis of *T. gondii* reveals that the parasite contains >20 species of sphingolipids consisting of both saturated and unsaturated fatty acids (Lige *et al.*, 2011). The parasite is capable of the de novo synthesis of sphingolipids, based on inhibitor studies (Sonda *et al.*, 2005), as well as on metabolic labeling studies of extracellular or released intracellular parasites (Azzouz *et al.*, 2002; Bisanz *et al.*, 2006). Despite its ability to generate sphingolipids, the parasite also appears to scavenge sphingolipids derived from the host cell via the host Golgi (de Melo and De Souza, 1996; Bisanz *et al.*, 2006).

In this article, we explored the interaction between the *T. gondii* PV and the host Golgi apparatus. We investigate the process of host sphingolipid delivery to the PV from the host Golgi and evaluate the importance of host-derived sphingolipids for parasite growth. Because current treatment options to fight toxoplasmosis are limited and poorly tolerated (Luft and Remington, 1992; Suzuki, 2002), defining the molecular basis by which sphingolipids contribute to *T. gondii* infections might inspire new drug treatments.

RESULTS

T. gondii actively scavenges exogenously derived ceramides from the host Golgi

Short-chain ceramides added exogenously to mammalian cells are internalized and, after 10 min, become concentrated in the Golgi apparatus (Lipsky and Pagano, 1985). Within the Golgi, ceramide is converted into sphingolipids (e.g., sphingomyelin or glucosylceramide), which may then be delivered to the plasma membrane via Golgi-derived, Rab-associated vesicles (Pagano *et al.*, 1991). A previous study reported that the obligate intracellular parasite *T. gondii* scavenges a fluorescently labeled analogue of ceramide from the host Golgi (de Melo and De Souza, 1996). We extended these observations by analyzing the time course of ceramide scavenging by *T. gondii* and the incorporation of this lipid into organelles of the parasite.

First, uninfected fibroblasts were incubated with NBD C6-ceramide and viewed by fluorescence microscopy. The results in Figure 1A confirm that within 10 min of exposure to NBD C6-ceramide the fluorescent lipid accumulated in the Golgi complex of the fibroblasts. A progressive redistribution of the fluorescence signal from the Golgi to the cell surface was observed over the time course of 20 min to 2 h (Figure 1A).

Next fibroblasts were infected with *T. gondii* for 24 h and then incubated with NBD C6-ceramide for 10 min. These infected cells showed an intense staining of the host Golgi, as was observed in uninfected cells (Figure 1B). After 20 min, the interior of the PV became fluorescent (Figure 1B, 20′ inset) and the parasite's plasma membrane displayed a weak labeling (Figure 1B). Over time the staining of the parasite intensified, and after 1 h the parasite's plasma membrane was brightly fluorescent. The apical region of the parasite that houses the Golgi complex and faces outward toward the PV membrane was also labeled (Figure 1B, 60′ inset), suggesting that the NBD-labeled lipids were redistributed within the parasite. Of interest, in infected cells the host Golgi remained brightly fluorescent after 2 h, whereas in uninfected cells the fluorescence signal was predominantly redistributed to the plasma membrane. This result suggests that the presence of the parasite may be slowing down or altering Golgi activities. Finally, egressing parasites still contained NBD-labeled lipids (Figure 1B, 120′ inset).

Our data confirm that *T. gondii* scavenges NBD C6-ceramide from the host Golgi. To determine whether the parasite is actively involved in the uptake of host Golgi–derived sphingolipids, we treated infected cells with pyrimethamine before incubating them with labeled ceramide; pyrimethamine is an inhibitor of the parasite's dihydrofolate reductase and acts to slow down parasite metabolism. In pyrimethamine-treated cells, the PVs contained dying parasites that displayed abnormal morphologies (Figure 1C, phase-contrast images). Treatment of infected cells with pyrimethamine abolished the fluorescence labeling of the parasite in a dose-dependent manner, indicating that an active parasite metabolism was required for the scavenging of lipids from the host Golgi.

To examine whether the parasites contained lipids derived from NBD C6-ceramide, we isolated parasites and analyzed their lipids by TLC. Fibroblasts were infected for 48 h and then incubated for either 1 or 6 h in the presence of NBD C6-ceramide. Total lipids were extracted from the egressed parasites and separated by TLC, and the NBD-containing lipids were visualized by fluorometry (Figure 1D). In addition to NBD C6-ceramide, other molecular species of NBD-labeled lipids were detected, with at least four distinct lipids discernible after 6 h of incubation (Figure 1D). The nature of these lipids remains to be identified, but lipids migrating between ceramides and sphingomyelin are usually glycosphingolipids, which abound in *T. gondii* (Azzouz *et al.*, 2002). No band corresponding to sphingomyelin was visible on the TLC plates under our experimental conditions. Thus the parasite either uses ceramides retrieved from the host Golgi to manufacture its own sphingolipids and/or is able to scavenge complex sphingolipids directly from the host Golgi.

The parasite attracts the host Golgi early during infection

Our data indicate that *T. gondii* localizes near the host Golgi apparatus and exploits the lipid content of this organelle (Figure 1A; de Melo and De Souza, 1996). Because this interaction is already clearly established at 24 h postinfection (p.i.), we next analyzed the distribution of the host Golgi apparatus relative to the PV at early times during an infection and assessed any physical transformations of this organelle. VERO cells were infected with *T. gondii* for 1, 2, 4, and 8 h and examined by fluorescence microscopy to compare the location of the Golgi and the PV; the host Golgi was visualized using antibodies against the *cis*-Golgi protein giantin, whereas the PV was identified using antibodies against the PV membrane protein GRA7.

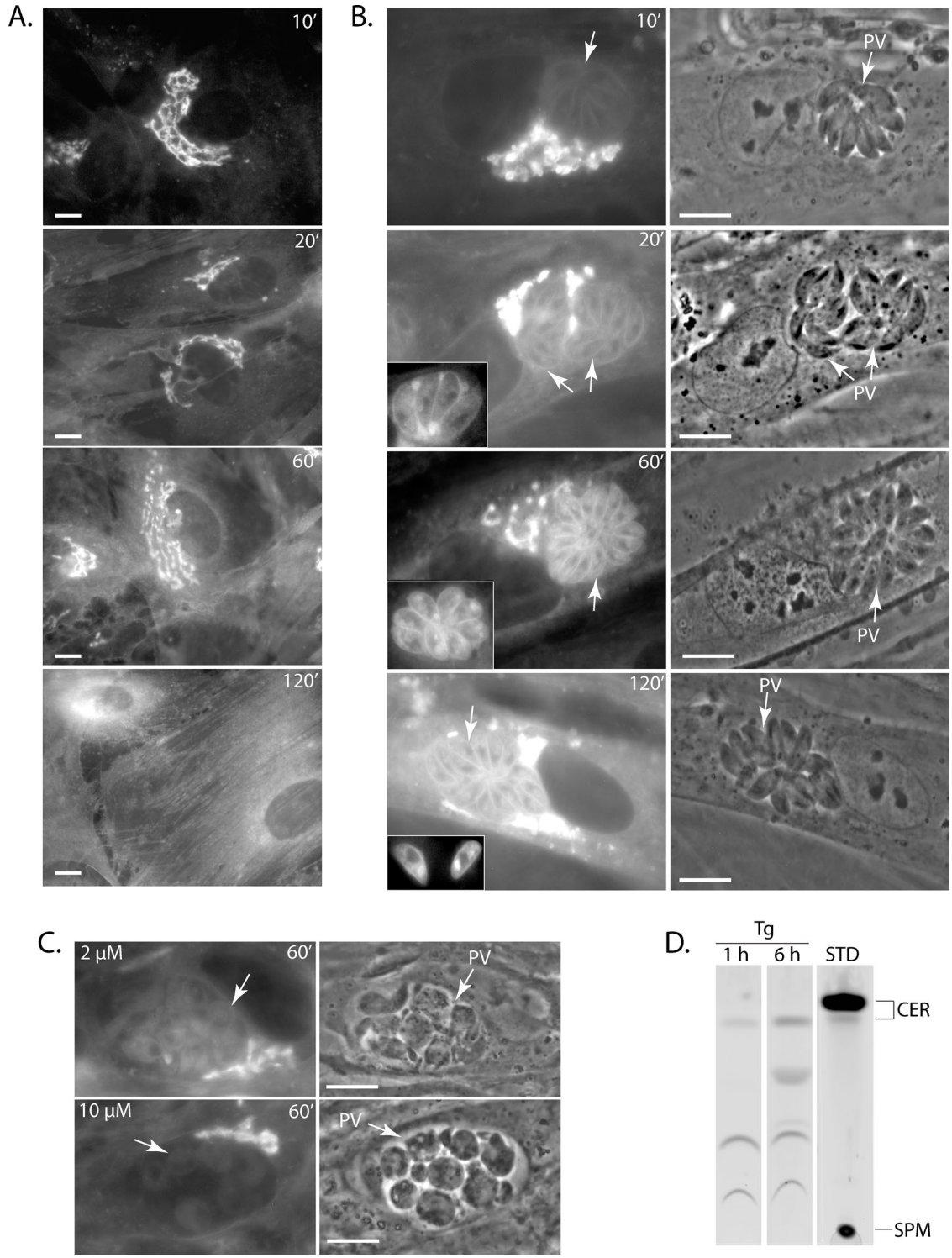

FIGURE 1: Association of host ceramides with the PV. (A) Live fluorescence microscopy of uninfected HFFs incubated with 5 µM NBD C6-ceramide complexed to BSA at the times indicated. (B) Live fluorescence microscopy of HFFs infected with *T. gondii* for 24 h and incubated with fluorescent ceramides as described in A. The arrows denote PVs. The insets of time points 20 and 60 min show additional parasites stained with NBD C6-ceramide, and the inset for the 120-min time point shows freshly egressed parasites. (C) Live fluorescence microscopy of HFF cells infected with *T. gondii* for 24 h and then treated with either 2 or 10 µM pyrimethamine for 24 h before the addition of fluorescent ceramide for 1 h. Arrows indicate PVs. (D) TLC plates of *T. gondii* lysates (Tg) revealed by fluorometry. Intracellular parasites were loaded with NBD C6-ceramide for 1 or 6 h and isolated from host cells, and their total lipids were extracted and fractionated by TLC as described in *Materials and Methods*. Fluorescence standards (STD) are shown in the right lane. CER, ceramides; SPM, sphingomyelin. Scale bars, 5 µm.

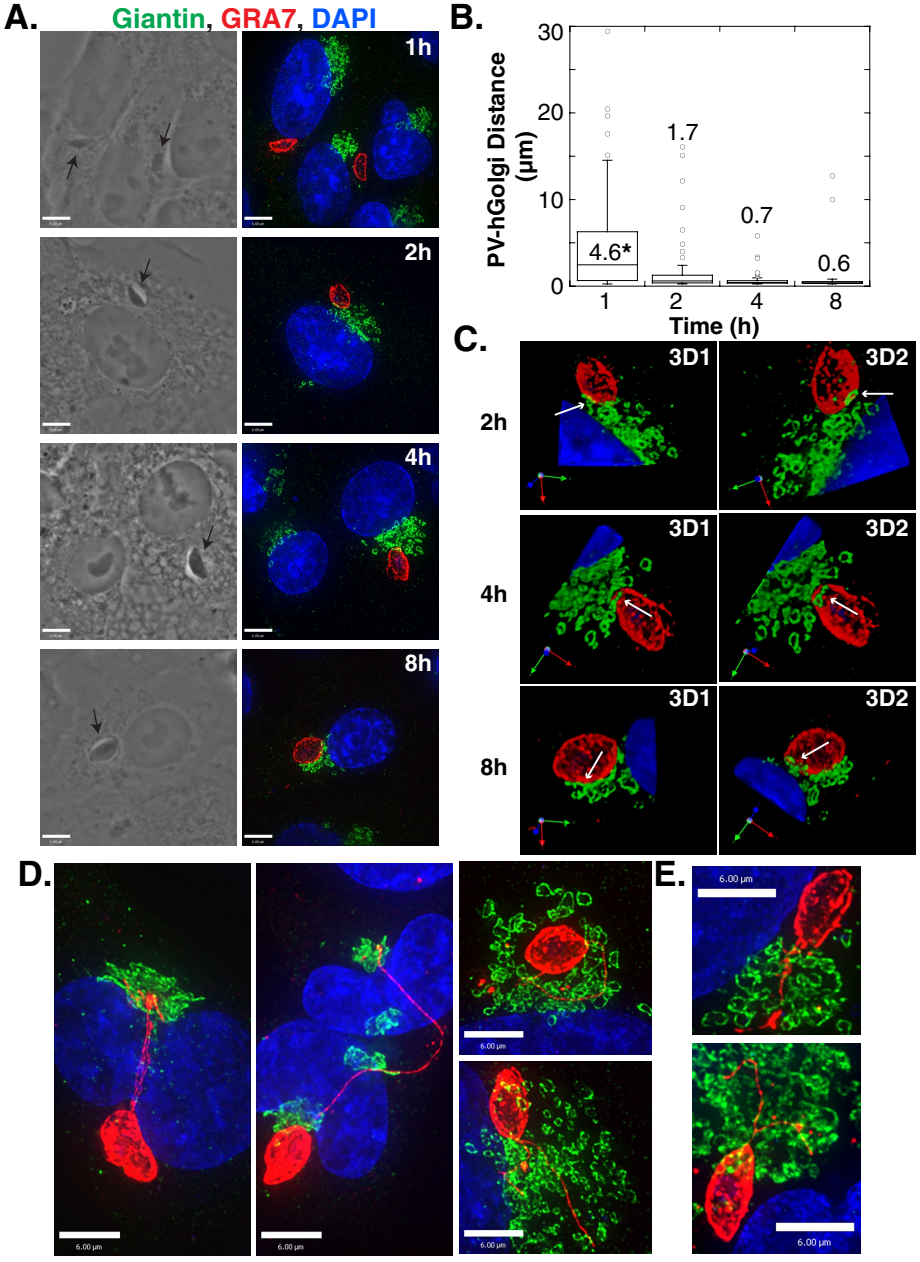

FIGURE 2: Attraction of the *T. gondii* PV for the host Golgi. (A) VERO cells were infected with *T. gondii* for the times indicated, fixed, and stained with 4′,6-diamidino-2-phenylindole (DAPI; blue, nucleus) and antibodies against giantin (green, Golgi) and GRA7 (red, PV). Representative extended focus images are shown. The arrows in the phase images point to the intracellular parasite. (B) Box plot showing the distribution of distances between the PV and the nearest part of the host Golgi. The data are from three independent experiments, and the total number of PV–giantin distances measured for the time points shown is 84, 70, 74, and 112, respectively. Whiskers of the box plots represent the upper and lower values excluding outliers, outliers are marked as open circles, and the line inside the box is the median value. The numbers written within the plot are the mean distances in micrometers. *$p < 0.001$. (C) 3D reconstructions of optical *z*-slices from the images in A. Arrows show PV–Golgi interaction. (D) HeLa cells were infected for 8 h, fixed, and stained as in A. (E) VERO cells were infected for 4 h, fixed, and stained as in A. Scale bars, 6 μm.

The PV preferentially localized close to the host Golgi within the first few hours of infection (Figure 2A). To quantify the association between the PV and host Golgi, we measured the closest distance between the two structures on three-dimensional (3D) volumes reconstructed from optical *z*-slices. At 1 h p.i., the distance between PVs and the host Golgi ranged (excluding outliers) from 15 to <1 μm, with 31 ± 4% of the PV population located within 1 μm of the host Golgi (Figure 2B). The percentage of PVs found <1 μm from the host Golgi increased from 69 ± 3% at 2 h p.i. to 89 ± 7 and 100% at 4 and 8 h p.i., respectively. For these PVs, sections of the host Golgi closely aligned with the edge of the PV as observed in 3D reconstructions of optical *z*-slices obtained from infected cells (Figure 2C). In some cases, the host Golgi appeared to extend on top of the PV (Figure 2C, 4-h time point) while the host Golgi partially surrounded the PV in other cells (Figure 2, A and C, 8-h time point). The close association of the PV and host Golgi did not appear to change the morphology of the Golgi at early times during an infection (Figure 2).

The physical attraction between the PV and host Golgi was further suggested by the observation that extensions of the PV membrane appeared to target the host Golgi. In a dramatic example, a PV distant from the host Golgi was connected to this organelle via several PV membrane (PVM) projections (PVMPs) that surrounded the host nucleus to reach the Golgi (Figure 2D). Impressively, in dividing cells harboring many sets of newly formed Golgi complexes, the PVMPs were observed threading through the host Golgi (Figure 2, D and E).

These results suggest that *T. gondii* is attracted to the host Golgi at the onset of infection and forms a close association with this host organelle.

The *T. gondii* PV localizes near the host Golgi before the host MTOC in nonpolarized cells

In nonpolarized cells, the MTOC is involved in positioning the Golgi apparatus in the perinuclear region (Kupfer *et al.*, 1982). Because we showed that the PV closely associates with the host Golgi by 2 h p.i. (Figure 2B), we addressed the question of whether the parasite first hijacks the host MTOC to recruit host microtubules and attract organelles such as the Golgi. Previous studies showed that the host MTOC detaches from the nuclear envelope, relocates to the PV surface at 24 h p.i., and remains associated with the PV until the end of the infection (Coppens *et al.*, 2006; Romano *et al.*, 2008; Walker *et al.*, 2008; Wang *et al.*, 2010). To clarify the sequence of these postinvasion events, we compared the timing of the PV–host MTOC recruitment with the timing of the PV–host Golgi association. We used immunofluorescence assays to detect the host MTOC and PV using antibodies against γ-tubulin and GRA7, respectively, and measured the distance between these structures from 2 until 24 h p.i. (Figure 3A). The mean distance between the PV and

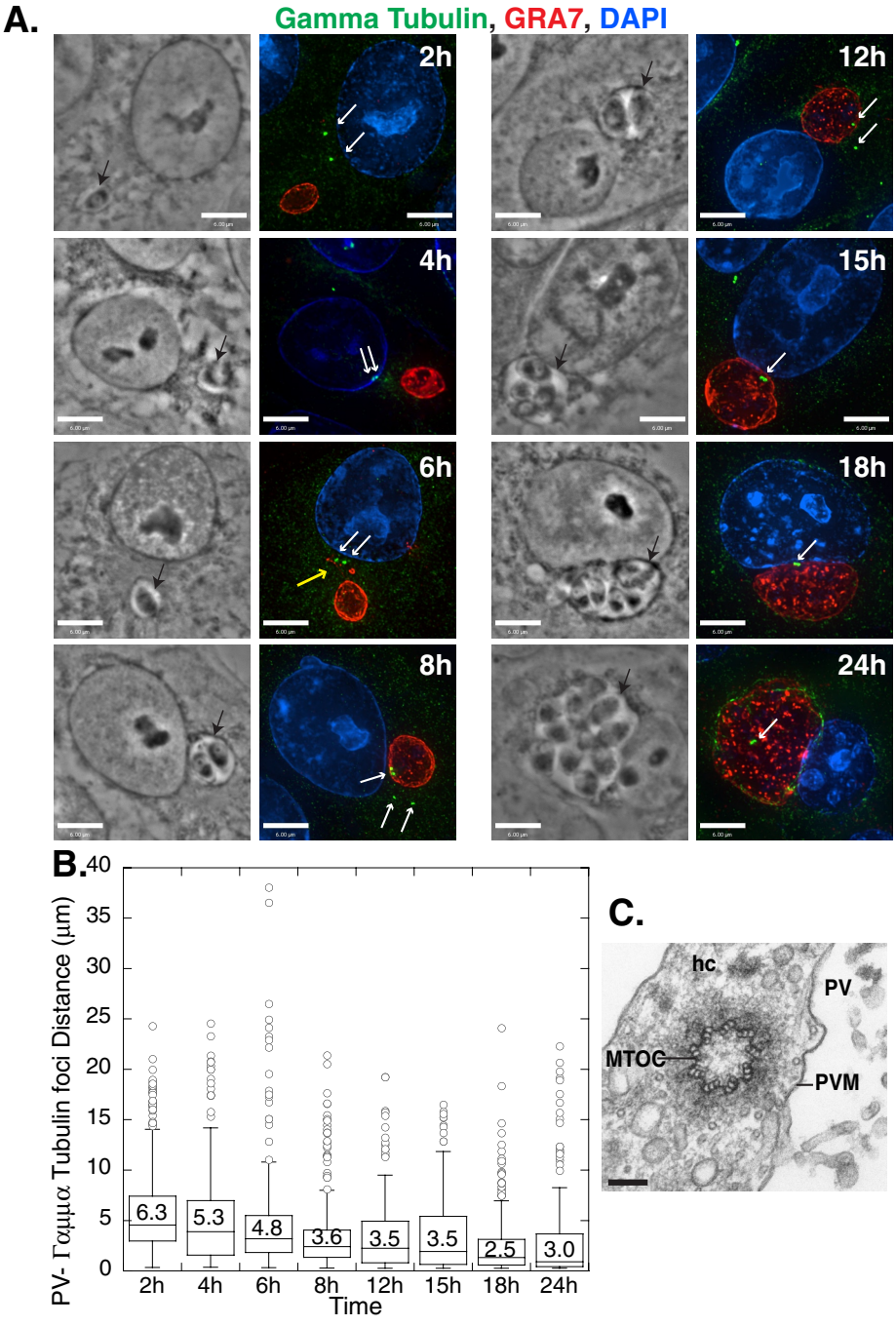

FIGURE 3: Localization of the *T. gondii* PV near γ-tubulin foci during an infection. (A) VERO cells were infected with *T. gondii*, fixed, and stained with DAPI (blue, nucleus) and antibodies against γ-tubulin (green, MTOC) and GRA7 (red, PV). Representative extended focus images are shown. Black arrows indicate the PV; white arrows denote the MTOCs. The yellow arrow indicates a PVMP. (B) Box plot (as in Figure 2) showing the distribution of distances between the PV and host γ-tubulin foci at the times indicated. The data are from three independent experiments, and the total number of PV–host γ-tubulin distances measured for the time points shown is 277, 235, 248, 318, 228, 189, 292, and 205, respectively. Scale bars, 6 μm. (C) Electron micrograph taken from a fibroblast infected with *T. gondii* for 36 h, showing a transverse section of the host MTOC near the PV on the right side. hc, host cell. Scale bar, 100 nm.

host γ-tubulin foci decreased between 2 and 8 h of infection, reaching a plateau between 8 and 12 h p.i. (Figure 3B). Of interest, this plateau coincides with the commencement of parasite replication within its PV (Figure 3A). As was observed with the host Golgi (Figure 2, D and E), PVMPs were sometimes seen extending toward the host MTOC (Figure 3A, 6-h time point). The percentage of PVs located within 1 μm of the γ-tubulin foci increased up to 24 h p.i., with 5 ± 1, 16 ± 5, 35 ± 9, and 52 ± 3% of the PVs close to the foci at 2, 8, 15, and 24 h p.i., respectively. These results contrast with the findings for the host Golgi–PV association, for which 69 ± 3% of the PVs were close to the *cis*-Golgi at 2 h p.i (Figure 2B). These results suggest that the PV associates with the host Golgi before localizing near the host MTOC.

As in previous studies, we frequently observed supernumerary centrosomes in infected cells, which correlates with the rupture of the nucleus–centrosome connection (Figure 3A, 8-h time point; Walker *et al.*, 2008). To verify the closeness of the host MTOC and the PV, we undertook ultrastructural studies in cells infected for 36 h. Transmission electron microscope (EM) observations show that the host MTOC was located distant from the host nucleus and was closely apposed to the PV membrane (Figure 3C and Supplemental Figure S1A). Our EM studies also confirmed the presence of supernumerary centrosomes, with one infected cell containing up to eight MTOCs adjacent to the PV (Supplemental Figure S1B).

The mammalian MTOC is composed of a pair of centrioles and a pericentriolar matrix. To determine whether an infection with *T. gondii* affects the composition of the MTOC, we examined the localization of additional components of this structure: NEDD1, a component of the γ-tubulin ring complex that is critical for microtubule nucleation, and pericentrin, a pericentriolar matrix protein. To track NEDD1, we transfected cells with NEDD1–green fluorescent protein (GFP) and then infected them with *T. gondii* for 18 h. The NEDD1-GFP foci localized along the edge of the PV and colocalized with γ-tubulin foci (Figure 4A). Because both γ-tubulin and NEDD1 are found in the γ-tubulin ring complex, we analyzed the localization of pericentrin. *T. gondii*–infected cells were stained with antibodies against pericentrin to assess the distance of pericentrin foci from the PV. Data show that the PV localized near host pericentrin foci during the infection; the anti-pericentrin antibody displayed a diffuse staining pattern within the parasites, but the pericentrin staining in the host cell was easily distinguishable (Figure 4B). The mean distance between PVs and the host pericentrin foci decreased between 4 and 8 h p.i. and then plateaued after 8 h (Figure 4C), as observed with the γ-tubulin foci (Figure 3B). The pericentrin and γ-tubulin foci colocalized at the edge of the PV (Figure 4D). These

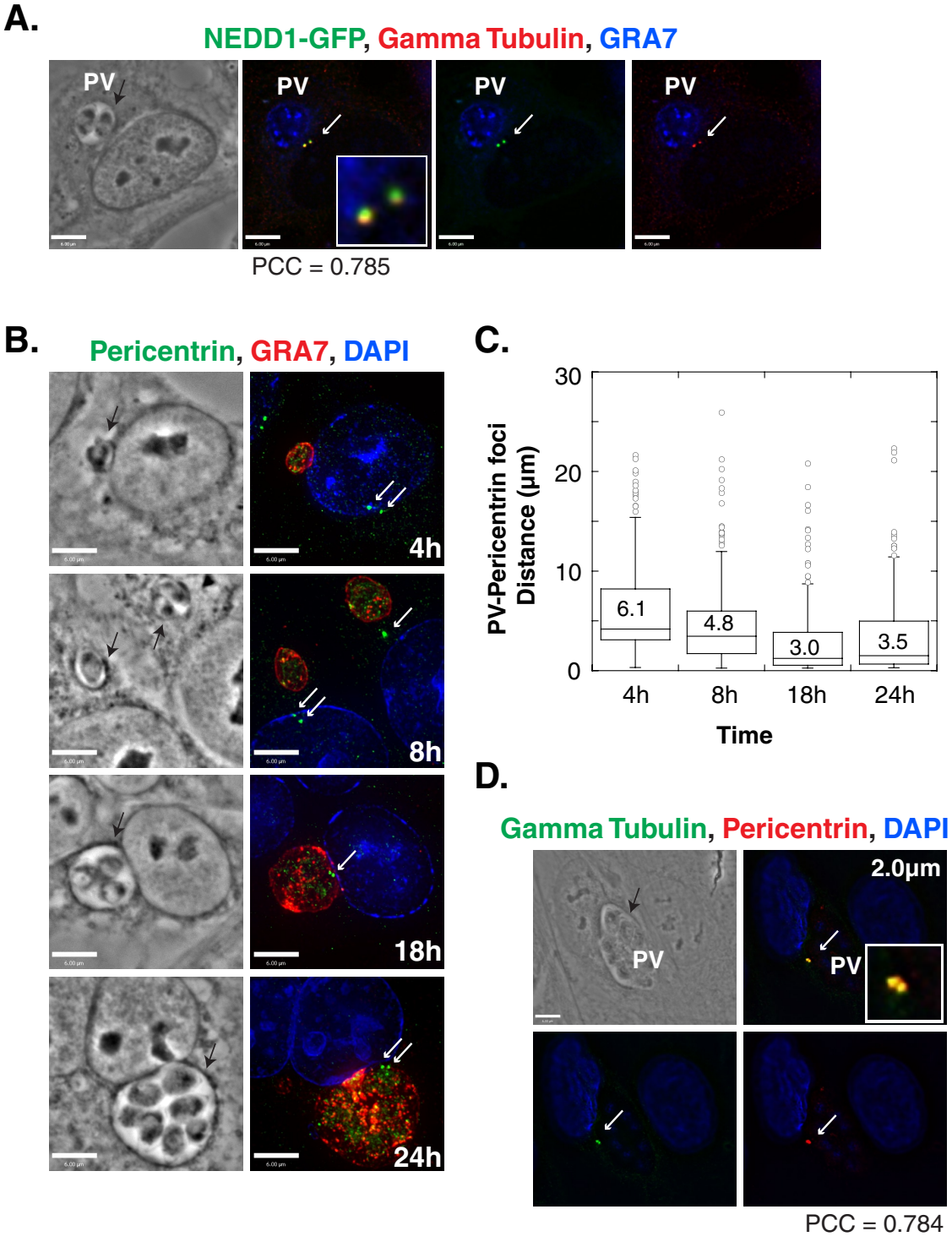

FIGURE 4: Localization of the *T. gondii* PV near the MTOC during an infection. (A) HeLa cells expressing NEDD1-GFP were infected with *T. gondii* for 18 h, fixed, and stained with antibodies against GRA7 (blue) to detect the PV and γ-tubulin (red). An individual *z*-slice is shown. (B) VERO cells were infected with *T. gondii* for the times indicated, fixed, and stained with DAPI (blue) and antibodies against pericentrin (green) and GRA7 (red). Representative extended focus images are shown. (C) Box plot (as in Figure 2) showing the distribution of distances between the PV and host pericentrin foci. The data are from three independent experiments, and the total number of PV–host pericentrin distances measured per time point shown is 202, 173, 177, and 193, respectively. (D) VERO cells were infected with *T. gondii* for 24 h, fixed, and stained with antibodies against γ-tubulin (green) and pericentrin (red). A single *z*-slice is shown. The PV is indicated by an arrow; PCC, Pearson *r*. Black arrows indicate the PV and white arrows the MTOC. Scale bars, 6 µm.

results reveal that in infected cells, the MTOCs that are recruited by *T. gondii* maintain their integrity, as they consist of centrioles surrounded by a pericentriolar matrix.

In polarized cells, the *T. gondii* PV also localizes near the host Golgi before the host MTOC

In nonpolarized cells the Golgi localizes in the perinuclear region near the MTOC, but in polarized Madin–Darby canine kidney (MDCK) cells the organization of the Golgi and MTOC is more complex. On differentiation, the centrioles migrate to the apical domain and are closely apposed to the apical membrane, where they do not nucleate many microtubules (Bacallao *et al.*, 1989). The Golgi is initially a compact structure located in the perinuclear region, but after differentiation the Golgi spreads around the nucleus in the apical region of the cell (Bacallao *et al.*, 1989). To determine whether the organization of the Golgi and centrioles in polarized MDCK cells affected the ability of the parasite to associate with these host structures or the timing of the interactions, we infected MDCK cells with *T. gondii* for 2 or 24 h and viewed the cells by fluorescence microscopy; we detected the PV, Golgi, and MTOC using antibodies directed against GRA7, giantin, and γ-tubulin, respectively (Figure 5 and Supplemental Figure S2). Early during infection, at 2 h p.i., the host γ-tubulin foci localized to the apical side of the nucleus, whereas the PV was adjacent to the nucleus (Figure 5A). On numerous occasions, a PV that was localized adjacent to the nucleus draped over the apical side of the nucleus and extended a PVMP or GRA7-positive vesicle toward the γ-tubulin foci (Figure 5A and Supplemental Figure S2A, yellow arrows). Later in infection, at 24 h p.i., the host MTOC was closely associated with large PVs. In these cases, the γ-tubulin foci were relocalized to the apical side of the PV as opposed to the apical side of the host nucleus. In sharp contrast, elements of the host Golgi were very closely associated with the edge of the PV membrane starting at 2 h p.i (Figure 5B and Supplemental Figure S2B). In some cases, the host Golgi surrounded the PV even at this early time point (Supplemental Figure S2B), and Golgi elements were observed to encircle PVMPs (Supplemental Figure S2C). At 24 h p.i., PVs were entirely encompassed by Golgi material, and the giantin material was very tightly associated with the PVM (Figure 5C). These observations indicate that in polarized MDCK cells, the PV first associates closely with the host Golgi and subsequently interacts with the host MTOC, which complements our results with nonpolarized cells. Of interest, in MDCK cells the attraction between the PV and host Golgi is more dramatic than in the nonpolarized cells that were analyzed.

The host Golgi is fragmented in infected cells, and the scattered Golgi ministacks distribute around the PV

We extended our studies on the PV–host Golgi association by assessing the morphology of the Golgi at later times during an infection. Early during an infection, regions of the host Golgi closely apposed the PV membrane, but the Golgi retained its perinuclear localization and compact structure (Figure 2, A and C). By 24 h p.i., the host Golgi often encompassed the PV, and the ribbon-like morphology of the Golgi was less distinct (Figure 1B). To further analyze the Golgi morphology, we infected VERO cells with *T. gondii* for 24 and 32 h and visualized the Golgi by immunofluorescence using antibodies against the *cis*-Golgi protein giantin (Figure 6A). In cells infected with *T. gondii* for 24 h, the structure of Golgi was less compact and more diffuse than in uninfected cells (Figure 6A). In some cases, the Golgi was disrupted into small, giantin-positive foci that were distributed around the PV (Figure 6A). The Golgi fragmentation was more pronounced at 32 than at 24 h p.i. (Figure 6A).

To quantify the level of Golgi fragmentation, we measured the number and volume of host giantin foci in infected cells at 32 h and compared the results to those for uninfected cells. The number of host giantin foci in infected cells significantly increased by sixfold over uninfected cells (Figure 6B), and the volume of these foci decreased significantly by 14-fold (Figure 6C). The breakdown of the host Golgi was independent of the host cell type, as the event also occurred in infected human foreskin fibroblast (HFF) and MDCK cells (Supplemental Figure S3). The attraction of the host Golgi by *T. gondii* is not a result of the expanding size of the PV, but instead seems to be an intrinsic component of the parasite's infectivity program. First, the host Golgi associates with the PV before parasite replication begins when the PV is still small in size (Figure 2A). Second, the PV of the related parasite *Plasmodium yoelii* does not have any physical contact with the host Golgi even if this parasite forms very large schizonts in liver cells (Supplemental Figure S3C).

In infected cells, the presence of supernumerary centrosomes appears to interfere with cytokinesis, as some infected cells contain multiple nuclei (Walker *et al.*, 2008). To determine whether the number of host nuclei was related to Golgi fragmentation, we compared fragmentation in infected cells with one or two host nuclei. We observed no difference in Golgi fragmentation between the two populations of infected cells (Supplemental Figure S4).

Up to this point, we focused on the fate of the *cis*-Golgi during a *T. gondii* infection since we followed the localization of the giantin protein. To determine whether the entire Golgi complex associates with the PV and is fragmented into smaller foci in infected cells, we examined the localization of the *trans*-Golgi network (TGN) protein golgin97 by immunofluorescence. We observed that the TGN also associated with the PV (Figure 6, D and E) and fragments into smaller golgin97-positive foci (Figure 6E). By following both compartments in the same infected cell, we observed that both the giantin- and golgin97-positive foci were distributed around the PV, but with little overlap between the two types of foci in infected cells displaying a dramatically disrupted Golgi complex (Figure 6E). The loss of overlap between giantin and golgin97 and the increase in Golgi fragmentation were more dramatic in infected cells containing large PVs, where the parasite had undergone numerous divisions (Figure 6E).

To analyze in finer detail the morphology of host Golgi fragments, we performed transmission EM studies in cells infected for 24, 36, and 48 h. In uninfected cells, the Golgi formed lateral stacks of long ribbons extending over 3 μm (Figure 7A, a). In infected cells, the typical organization of the Golgi was lost, but instead abundant shortened stacks made of four to six laterally linked cisternae were visible around the PVs (Figure 7A, b and c). These ministacks were not aligned with each other and had no particular orientation toward the PV. Some ministacks were very close to the PV membrane, albeit without any attachment to this membrane, and some were squeezed between host mitochondria attached to the PV membrane. To ascertain the origin of the ministacks, we performed immunogold staining using anti-giantin antibodies on cryosections of cells infected for 24 h (Figure 7B). As we expected, the ministacks were decorated with gold particles, indicating that giantin was maintained on the ministacks. In infected cells, there was an increase in the relative number of host Golgi elements detected by EM with a corresponding decrease in the relative size of these elements (Figure 7C). In cells infected for 24 versus 48 h, there was an increase in the number of Golgi elements, although without a significant difference in size (Figure 7C).

The structural alterations of the Golgi in *T. gondii*–infected cells might result from the modification of Golgi proteins, such as golgins

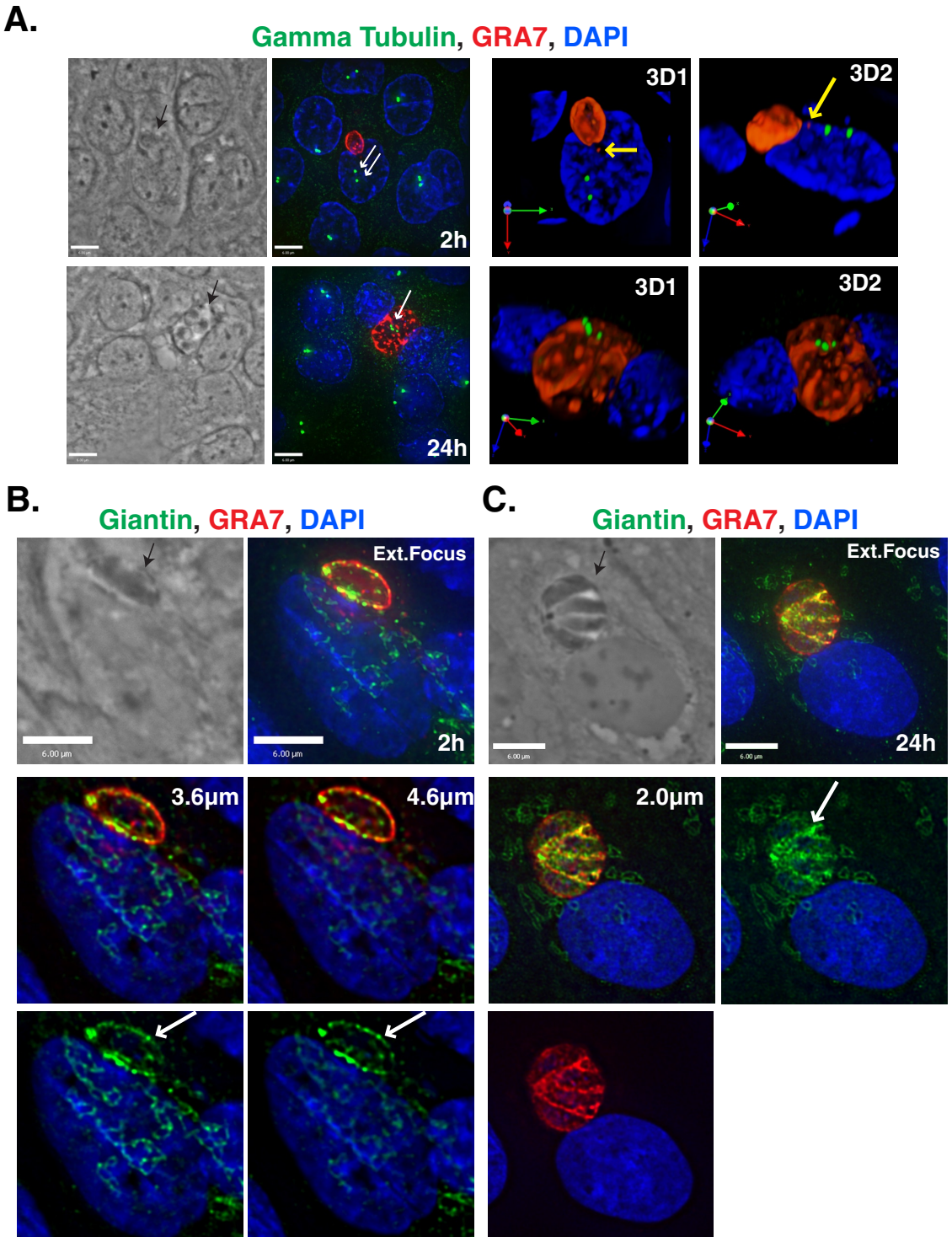

FIGURE 5: Localization of the *T. gondii* PV near the host Golgi before the host MTOC in MDCK cells. (A) MDCK cells were infected with *T. gondii* for 2 or 24 h, fixed, and stained with DAPI (blue) and antibodies against γ-tubulin (green) and GRA7 (red). The MTOC is indicated with a white arrow and PVs with the black arrow. The yellow arrows denote PVMPs extending toward the MTOC. Extended focus images are shown on the left next to the phase images. The panels labeled 3D are 3D reconstructions of the *z*-stacks. (B) MDCK cells were infected with *T. gondii* for 2 h, fixed, and stained with DAPI (blue) and antibodies against giantin (green) and GRA7 (red). Shown are an extended focus image, phase image, and two individual optical *z*-slices (3.6 and 4.6 µm). The white arrows indicate host Golgi elements that are closely associated with the PV, and the black arrows denote the PV. (C) MDCK cells were infected with *T. gondii* for 24 h and stained as in B. Shown are a phase image, extended focus image, and an individual *z*-slice (2.0 µm). The arrows are as described in B. Scale bars, 6 µm.

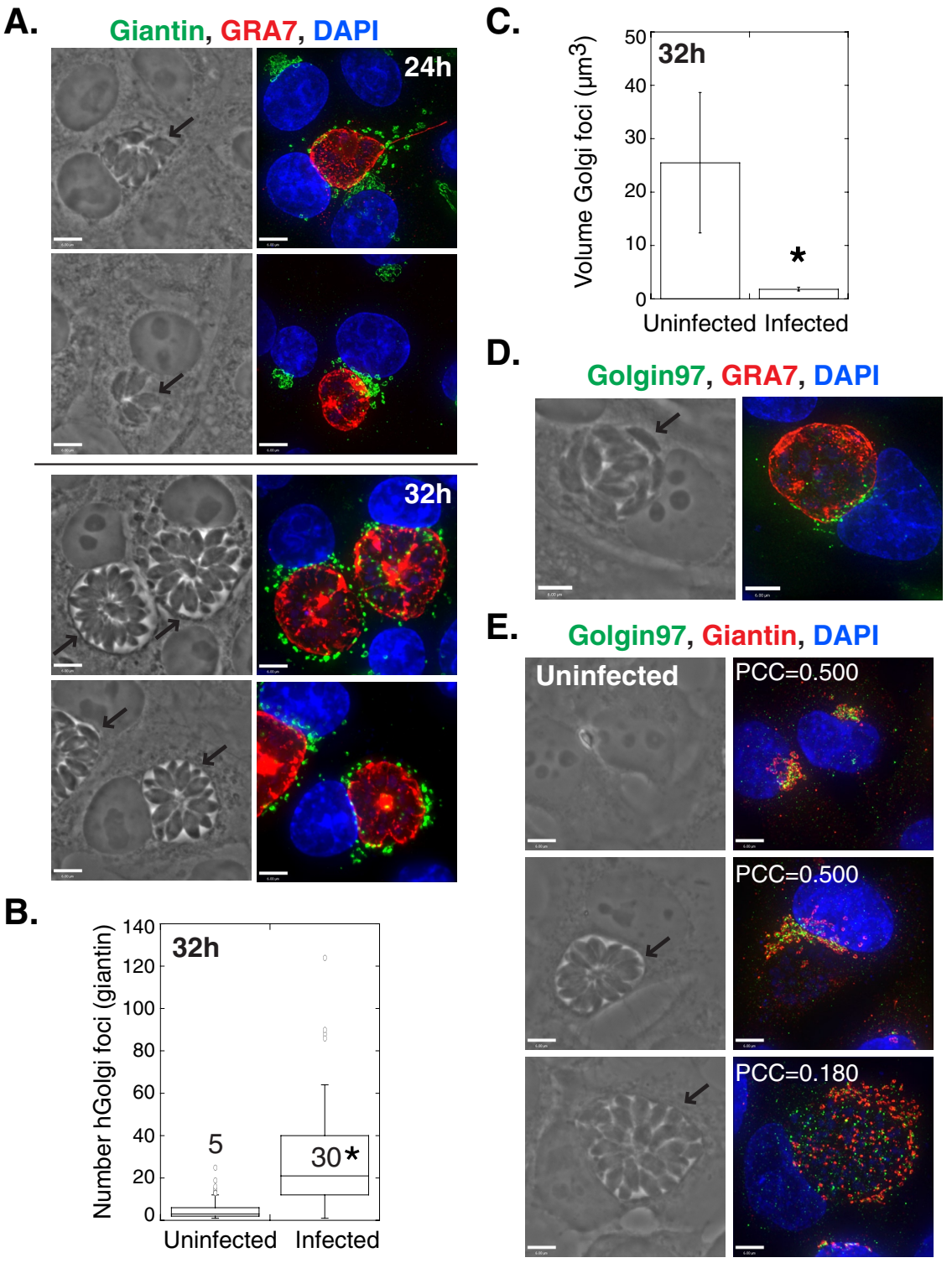

FIGURE 6: Remodeling of the host Golgi during a *T. gondii* infection. (A) VERO cells were infected with *T. gondii* for 24 or 32 h, fixed, and stained for fluorescence microscopy with DAPI (blue) and antibodies against giantin (green) and GRA7 (red). Representative extended focus images are shown, along with the corresponding phase images. (B) The number of giantin foci was measured as described in *Materials and Methods*. The box plot (as in Figure 2) shows the distribution of the number of host giantin foci from three independent experiments. The mean number of host Golgi foci is shown. *$p < 0.001$. (C) The mean volume of the host Golgi foci was measured as described in *Materials and Methods*. The mean volume was calculated from three independent experiments. Error bars, SD. *$p < 0.001$. (D) Representative phase and extended focus images of HeLa cells infected with *T. gondii* for 32 h, fixed, and stained with DAPI (blue) and antibodies against golgin97 (green) and GRA7 (red). (E) HeLa cells were infected with *T. gondii* for 32 h, fixed, and stained with DAPI (blue) and antibodies against golgin97 (green) and giantin (red). Representative phase and extended focus images are shown. PCC denotes the Pearson's *r*; black arrows indicate PVs. Scale bars, 6 μm.

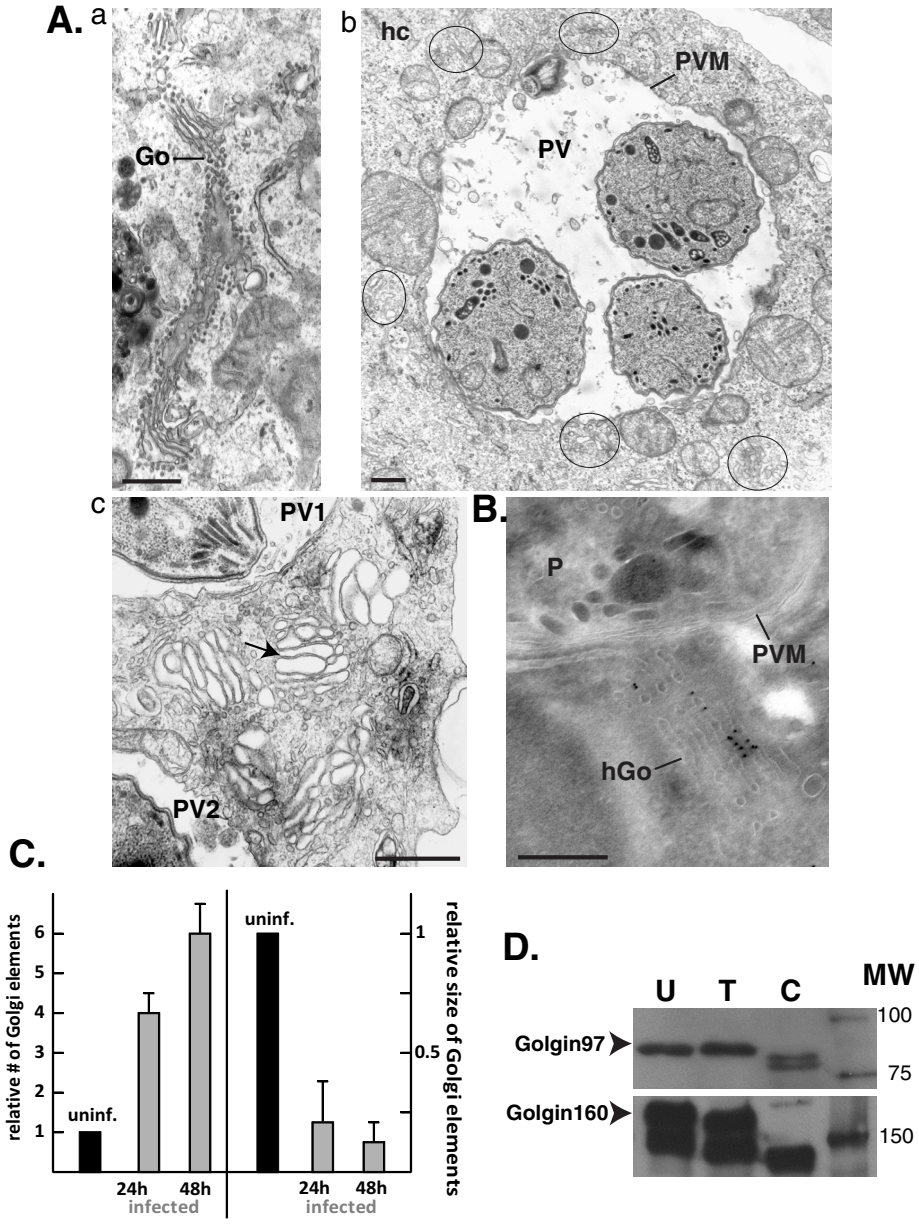

FIGURE 7: Fragmentation of the host Golgi into ministacks in infected cells. (A) EM of an uninfected VERO cell (a) or infected cells with *T. gondii* for 24h (b, c). In b, the fragments of the host Golgi surrounding the PV are encircled. In c, the arrow pinpoints a Golgi ministack between two PVs. (B) Immuno-EM of a HeLa cell infected with *T. gondii* for 24 h labeled with anti-giantin antibodies revealing the association of gold particles on a ministack close to the PV. P, parasite. Scale bars, 250 nm. (C) Quantification of EM observations. Comparison of the numbers and average sizes of Golgi elements in uninfected cells (uninf.) vs. infected cells for 24 and 48 h. Data show means ± SD of three independent experiments. (D) Cell lysates (50 µg) from uninfected (U), *T. gondii*–infected (30 h; T), and *C. trachomatis*–infected (30 h) HeLa cells were separated by SDS–PAGE. The Golgi proteins golgin97 and golgin160 were detected by immunoblotting, and the arrows pinpoint the full-length version of these proteins. MW indicates the molecular weight markers in kilodaltons.

(e.g., p115, golgin245, GM130), which contribute to the structural organization of this organelle (Barr and Short, 2003; Short *et al.*, 2005). For instance, during apoptosis or an infection with *Chlamydia trachomatis*, golgin proteins are proteolytically cleaved, leading to fragmentation of the Golgi (Mancini *et al.*, 2000; Chiu *et al.*, 2002; Lane *et al.*, 2002; Nozawa *et al.*, 2002; Lowe *et al.*, 2004; Heuer *et al.*, 2009). To determine whether the cleavage of host Golgi proteins occurs during a *T. gondii* infection, we examined by immunoblotting the status of golgin160 and golgin97, which localize to the *cis*-Golgi network and the TGN, respectively. Lysates from uninfected cells and *C. trachomatis*–infected cells were used as negative and positive controls, respectively. Neither golgin97 nor golgin160 was cleaved during a *T. gondii* infection, although both proteins were cleaved during an infection with *C. trachomatis* (Figure 7D).

Taken together, these data indicate that a *T. gondii* infection in mammalian cells induces the fragmentation of the Golgi into ministacks, which surround the PV. Ministack formation appears to be independent of the proteolytic cleavage of Golgi matrix proteins, at least as documented for golgin160 and golgin97.

The cystogenic Prugniaud strain of *T. gondii* also attracts, fragments, and scavenges ceramides from the host Golgi, although to a lesser extent than the RH strain

Our previous experiments on the host Golgi–PV interaction were performed using the RH strain of *T. gondii*, which is a highly virulent strain in mice (Dubey, 1977). We wanted to examine whether the Prugniaud strain of *T. gondii*, which is capable of forming cysts, behaves like the RH strain with regard to the ability to attract and remodel the host Golgi, as well as to scavenge sphingolipids from this organelle. In a preliminary series of experiments we compared the growth rate of these two parasite strains in vitro. HeLa cells were infected with each strain and inspected by microscopy to determine the number of parasites per PV (Figure 8A). At 24 h p.i., ~40% of PVs contained eight RH parasites, as opposed to less than ~10% of PVs for the Prugniaud strain. PVs containing more than eight parasites were only observed for the RH strain at this time point. This result was verified by [^{3}H]uracil incorporation assays to measure parasite replication in fibroblasts. Data indicate that the Prugniaud strain incorporated tritiated uracil at 10.4% of the rate of the RH strain ($p < 0.001$). In addition, we performed a plaque assay and measured the size of the lysed area in a cell monolayer infected by each strain (Figure 8B). Fibroblasts were infected with each strain and incubated for 7 d to allow for multiple rounds of replication and egress. The RH strain produced plaques that were significantly larger than those of the Prugniaud strain by about twofold (Figure 8B).

To compare the ability of the Prugniaud strain to attract the host Golgi, we infected HeLa cells for 24 h with either the Prugniaud or RH strain and visualized the host Golgi by immunofluorescence using antibodies against giantin. The majority of the PVs of the

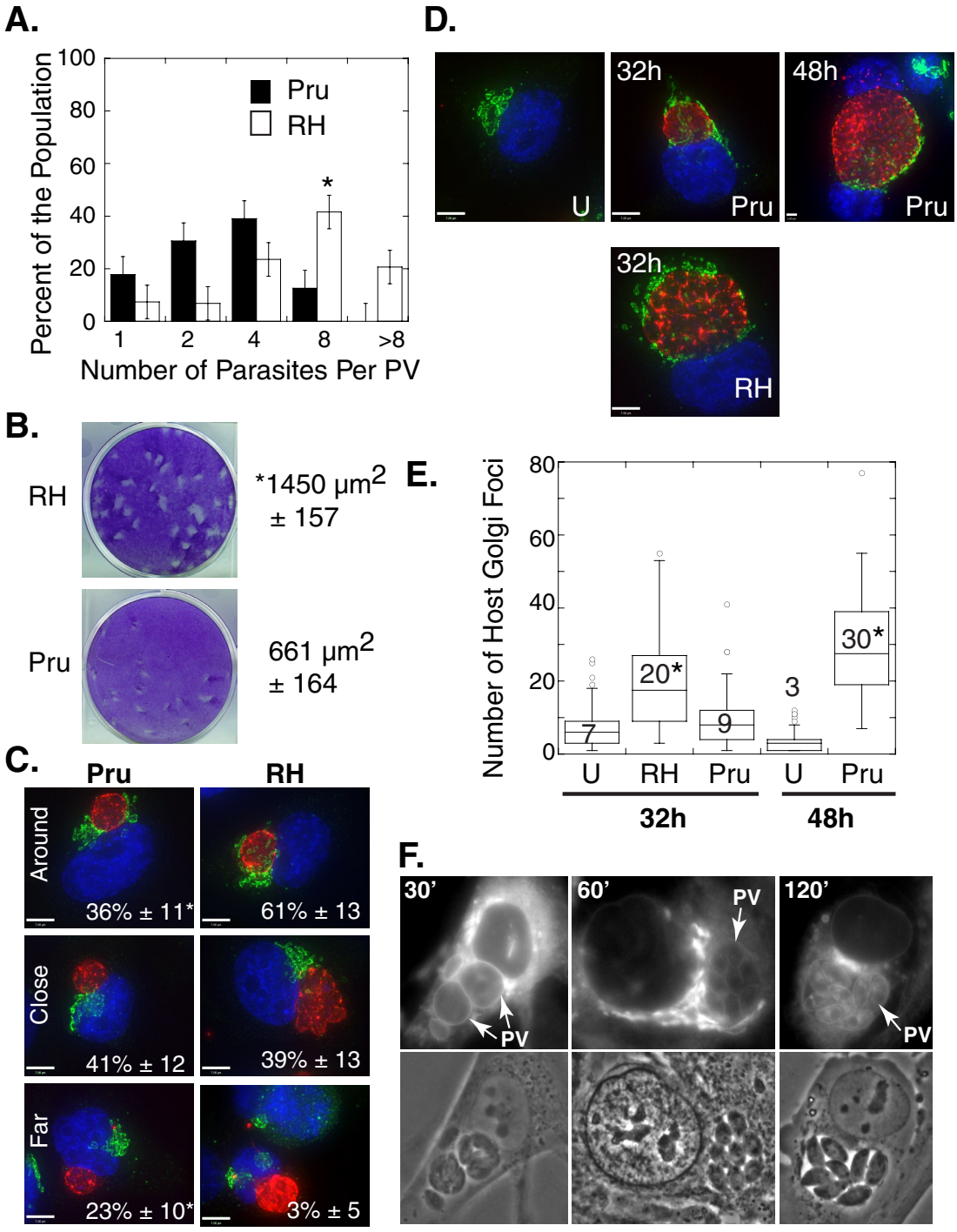

FIGURE 8: Distribution and morphology of the host Golgi in cells infected with the cystogenic *T. gondii* strain Prugniaud. (A) Distribution of the number of parasites per PV in HeLa cells infected with *T. gondii* RH (white) or Prugniaud (Pru, black) parasites for 24 h. Results in percentage are expressed as the mean number of intravacuolar parasites ± SE for three independent experiments. *$p < 0.05$. (B) Plaque assays were performed as described in *Materials and Methods*. The mean area of the plaques ± SD was calculated from three independent experiments. (C) HeLa cells were infected with *T. gondii* RH or Prugniaud parasites for 24 h, fixed, and stained with DAPI (blue) and antibodies against giantin (green) and GRA7 (red). The infected cells were grouped into three categories (around, close, and far), as described in *Materials and Methods*. The mean percentage of the population (± SD) was calculated from three independent experiments. *$p < 0.01$. (D) Uninfected (U) or *T. gondii* RH– or Prugniaud–infected HeLa cells were fixed and stained with DAPI (blue) and antibodies against giantin (green) and GRA7 (red). Representative extended focus images are shown. Most of the RH parasites egressed from their PV by 48 h of infection and are not shown. (E) The number of giantin foci was measured as described in *Materials and Methods* for uninfected (U), Prugniaud-infected (Pru), and RH-infected (RH) HeLa cells. The box plot (as described in Figure 2) shows the distribution of the number of host giantin foci from three independent experiments. *$p < 0.01$ (as compared with uninfected cells). (F) Live fluorescence microscopy of HFF cells infected with the *T. gondii* strain Prugniaud for 24 h and incubated in the presence of 5 μM NBD C6-ceramide complexed to BSA for the times indicated.

Prugniaud strain localized near the host Golgi (Figure 8C). There was, however, a delay in the PV–host Golgi association for the Prugniaud strain, since 23% of these PVs were still distant from the Golgi by 24 h, as opposed to only 3% of the RH PVs (Figure 8C). The Prugniaud strain was able to induce host Golgi fragmentation, but, as with its association with the Golgi, a delay was observed (Figure 8D). By 32 h p.i., the host Golgi was fragmented in RH-infected cells, but the structure of this organelle was more preserved in Prugniaud-infected cells (Figure 8D). Unlike in RH-infected cells, the number of host giantin-positive foci in cells infected with Prugniaud parasites for 32 h was similar to that of uninfected cells (Figure 8E). By 48 h p.i., however, the number of host giantin-positive foci increased by 10-fold in Prugniaud-infected cells (Figure 8E). These results indicate that during a Prugniaud infection the PV–host Golgi association and Golgi fragmentation occur but are delayed as compared with an RH infection. This delay might be related to the slower growth rate of the Prugniaud strain.

Because the cystogenic Prugniaud strain associated with the host Golgi, we assessed the ability of this strain to scavenge host sphingolipids. HFFs infected with Prugniaud parasites for 24 h were incubated with NBD C6-ceramide for 30 min, 1 h, and 2 h and then viewed live by fluorescence microscopy (Figure 8F). The host Golgi was brightly fluorescent at all time points, whereas the parasite was progressively stained on the PV membrane, on the parasite's plasma membrane, and finally within the parasite (Figure 8F). These results indicate that Prugniaud parasites were also capable of retrieving sphingolipids from the host Golgi, although the PV–host Golgi association and Golgi fragmentation were delayed in this strain compared with the RH strain.

Host sphingolipid levels affect *T. gondii* growth

We established that the host Golgi represents a source of sphingolipids for intravacuolar *T. gondii*. Next we sought to examine the reliance of *T. gondii* on host sphingolipids that are either produced by its host cell or present in the medium. To analyze the influence of host sphingolipids on *T. gondii* growth, we manipulated the levels of these lipids in the host cell and measured parasite grown using [^{3}H] uracil incorporation assays (Table 1). We targeted four major pathways for ceramide generation in mammalian cells from which the parasite may scavenge ceramides/sphingolipids: the pathways of de novo synthesis, neutral and acid sphingomyelinase activities, and uptake of extracellular ceramide (Figure 9).

First, we analyzed the effect of ceramides produced de novo in the host ER on *T. gondii* replication (Table 1). Treatment of infected cells with myriocin, an inhibitor of serine palmitoyltransferase that catalyzes the first step in sphingosine biosynthesis in the de novo pathway of ceramide synthesis, resulted in a significant decrease in parasite replication in a dose-dependent manner. We and another group (Pratt *et al.*, 2013) did not observe any deleterious effects of myriocin treatment on extracellular *T. gondii*. However, to confirm that the effect of parasite growth in cells exposed to myriocin is due to the inhibition of host serine palmitoyltransferase, we also monitored parasite replication in the mutant LY-B cell line, which is incapable of de novo sphingolipid synthesis due to a loss of serine palmitoyltransferase activity (Hanada *et al.*, 1998). Compared to the parental cell line CHO-K1, uracil uptake by the parasites was significantly reduced by twofold in LY-B cells (Table 1). The negative impact on parasite development from defects in host de novo sphingolipid synthesis suggests that *T. gondii* may also depend on the sphingolipid biosynthetic pathway of its host cell.

Second, we investigated the role of host neutral sphingomyelinases on parasite replication. Located at the plasma membrane of mammalian cells, neutral sphingomyelinases catalyze the release of ceramide from sphingomyelin in response to cellular stress (Wu *et al.*, 2010). We analyzed the effect of the noncompetitive inhibitor GW 4869 of neutral sphingomyelinases on the replication of *T. gondii*. A modest, dose-dependent decrease in uracil uptake was observed in infected cells treated with GW 4869 (Table 1). Third, we examined the contribution of host acid sphingomyelinases on parasite growth. The mutant cell NPD-A has a defect in acid lysosomal sphingomyelinases, and defects in these sphingomyelinases result in the accumulation of sphingolipids in late endosomes/lysosomes (Ng *et al.*, 2008). The growth of *T. gondii* in NPD-A cells was significantly enhanced, as a twofold increase in uracil uptake was measured in the mutant versus wild-type fibroblasts (Table 1).

Fourth, we probed the influence of excess ceramides added in the medium on parasite replication. In this case, parasite growth was significantly augmented in a dose-dependent manner (Table 1).

These observations indicate that host cell sphingolipid levels influence the development of *T. gondii*. They also suggest that the parasite may take advantage of the different sources of sphingolipids present in the cell and its scavenging of these lipids is not limited to sphingolipids present in the Golgi.

Condition	Parasite replication [^{3}H]uracil incorporation in cpm (% control)
	A. +Myriocin
0 μM	4990 ± 222
5 μM	3879 ± 199* (78%)
10 μM	2707 ± 88** (54%)
CHO-K1	5225 ± 125
LY-B	3003 ± 96** (57%)
	B. +GW 4869
0 μM	5001 ± 328
1 μM	4330 ± 287* (86%)
5 μM	4017 ± 120* (80%)
NHF	5419 ± 325
NPD-A	9528 ± 458** (176%)
	C. +Exogenous C6-ceramide
0 μM	5420 ± 280
5 μM	7002 ± 321* (130%)
15 μM	8160 ± 450** (150%)

Uracil incorporation assays to monitor *Toxoplasma* growth at 24 h p.i. Condition A probes the influence of host ceramide synthesis on parasite development in HFFs using myriocin at the indicated concentrations or in LY-B mutant cells. Condition B assesses the effect of host sphingomyelin degradation on parasite development in HFFs using GW 4869 at the indicated concentrations or in NPD-A mutant cells. Condition C monitors the effect of excess ceramide exogenously added in the medium at the indicated concentrations on *Toxoplasma* growing in HFFs. Data are means ± SD from three independent experiments (*$p < 0.05$; **$p < 0.01$).

TABLE 1: Influence of host ceramide levels on *Toxoplasma* growth.

Host Golgi–derived vesicles are intercepted by *T. gondii* and sphingolipids are transported to the PV via Rab14-, Rab30-, and Rab43-associated vesicles

The close association of *T. gondii* with the host Golgi may facilitate the scavenging of sphingolipids present in this organelle by the parasite. One possible mechanism that the parasite may employ to

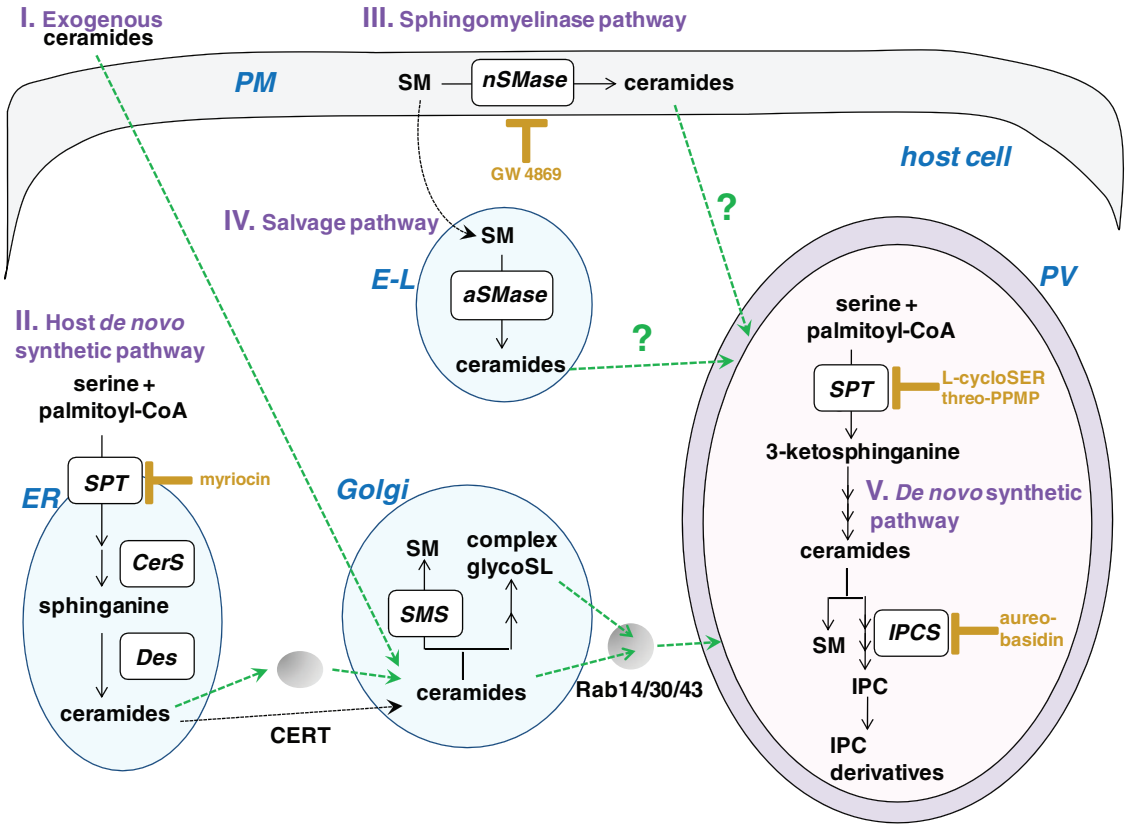

FIGURE 9: Sources of sphingolipids for the parasite. The biosynthetic pathways for sphingolipids in both the host cell and the parasite. (I) Ceramides added exogenously to mammalian cells are internalized and become concentrated in the host Golgi apparatus, where ceramides are converted into sphingomyelin (SM) or complex glycosphingolipids (glycoSL), which may then be delivered to the plasma membrane. (II) In the host de novo synthetic pathway, ceramides are produced in the ER. The inhibitor myriocin blocks serine palmitoyltransferase (SPT), which catalyzes the first step in the pathway (CerS, ceramine synthase; Des, dihydroceramide desaturase). Ceramides are then transferred to the Golgi either via vesicles or CERT. Within the Golgi, ceramides are converted into sphingomyelin by sphingomyelin synthases (SMS) or complex glycoSL. (III) In the sphingomyelinase pathway, neutral sphingomyelinase (nSMase) in the plasma membrane catalyze the hydrolysis of sphingomyelin to ceramides. The compound GW 4869 is a noncompetitive inhibitor of neutral sphingomyelinases. (IV) In the salvage pathway, acid sphingomyelinase located in the endolysosomes (E-L) catalyze the hydrolysis of sphingomyelin into ceramides. (V) The parasite has its own de novo synthesis pathway for ceramides and sphingomyelin, inositol phosphoceramide (IPC) by IPC synthase (IPCS), and IPC derivatives, based on metabolic labeling studies. Arrows in green are the potential host pathways that are diverted by *Toxoplasma*.

scavenge sphingolipids is to intercept host Rab-mediated vesicular transport from the Golgi. To investigate this possibility, we followed the distribution of Golgi-derived vesicles by focusing on those marked with Rab14, Rab30, or Rab43.

Rab14 mediates trafficking between the TGN, endosomes, and the plasma membrane (Junutula *et al.*, 2004; Proikas-Cezanne *et al.*, 2006; Kitt *et al.*, 2008). We examined the localization of host Rab14-associated vesicles in *T. gondii*–infected cells. In uninfected cells expressing GFP-tagged Rab14, the fluorescence signal localized to the Golgi as well as to vesicular structures as described previously (Junutula *et al.*, 2004; Figure 10A). The localization of the Rab14-GFP–associated vesicles changed dramatically in cells infected with red fluorescent protein (RFP)–expressing RH parasites (Figure 10B). Rab14-GFP that localized to the Golgi surrounded the PV, whereas numerous Rab14-GFP puncta concentrated at the periphery of the PV (Figure 10B). Viewing individual optical *z*-slices demonstrated that Rab14-GFP puncta were localized on top of the PV as well as inside the PV, either at the edge or in the middle of the vacuole (Figure 10B). At times the Rab14-GFP puncta were squeezed between parasites. To determine whether the cystogenic Prugniaud strain was also able to hijack host Rab14-associated vesicles, we infected cells expressing GFP-tagged Rab14 (Figure 10C). As with the RH strain, Prugniaud PVs were surrounded by Rab14-GFP, and some puncta were detected within the PV lumen. However, fewer intraluminal Rab14-GFP puncta were detected within the PV of the Prugniaud strain as compared with RH (Figure 10C).

Because the host Golgi apparatus is fragmented into ministacks in infected cells, we next wanted to examine whether the Rab14-GFP puncta colocalized with markers of the *cis*-Golgi (GRASP65) or the TGN (golgin97) and were then part of these ministacks. The level of colocalization between Rab14-GFP and the Golgi markers was calculated by determining the product of the differences from the mean (PDM; Figure 10, D and E). Rab14-GFP showed a strong colocalization around the PV with both GRASP65 and golgin97 (Figure 10, D and E). As observed previously, Rab14-GFP puncta distributed along the edge and within the PV lumen, as evidenced by a regular distribution of the fluorescence foci within

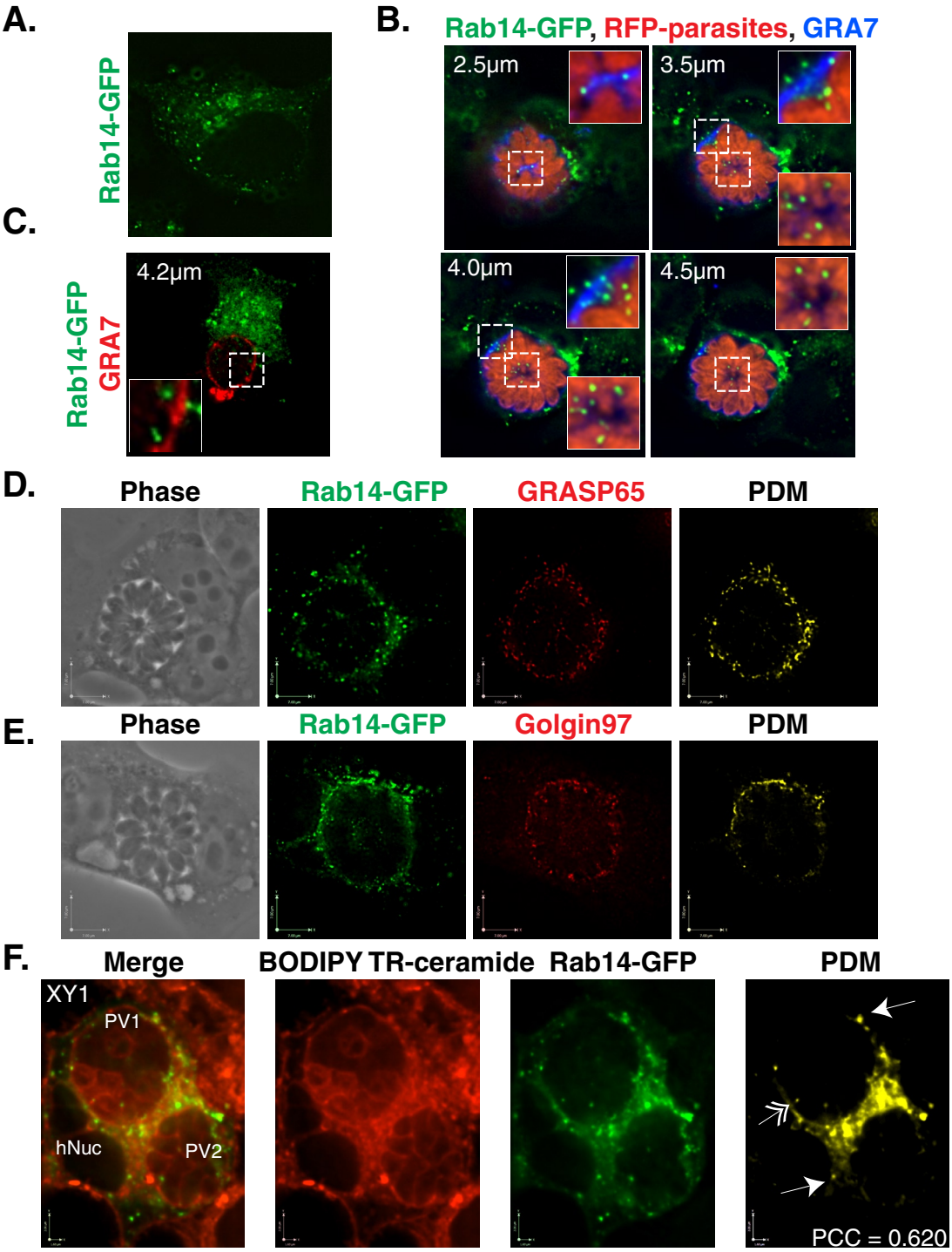

FIGURE 10: Interception of host Golgi–derived vesicles by *T. gondii*. (A) HeLa cells expressing Rab14-GFP (green) were fixed and viewed by fluorescence microscopy. An individual optical *z*-slice is shown. (B) HeLa cells expressing Rab14-GFP (green) were infected for 30 h with *T. gondii* RH parasites expressing RFP (red), fixed, and stained with antibodies against GRA7 (blue). Optical *z*-slices are shown. The inset is a magnified view of the boxed region. (C) HeLa cells expressing Rab14-GFP (green) were infected with cystogenic *T. gondii* Prugniaud parasites for 30 h, fixed, and stained with antibodies against GRA7 (red). Optical *z*-slices for two infected cells are shown. The inset is a magnified view of the boxed region. (D) HeLa cells expressing Rab14-GFP (green) were infected for 32 h with *T. gondii* RH, fixed, and stained with antibodies against GRASP65 (red). An optical *z*-slice is shown for the phase, Rab14-GFP, and GRASP65 channels plus the positive PDM. (E) HeLa cells expressing Rab14-GFP (green) were infected for 32 h with *T. gondii* RH, fixed, and stained with antibodies against golgin97 (red). An optical *z*-slice is shown for the phase, Rab14-GFP, and golgin97 channels plus the positive PDM. (F) HeLa cells expressing Rab14-GFP (green) were infected with RH parasites for 30 h and incubated in the presence of BODIPY TR C5-ceramide (red) for 40 min. An optical *z*-slice is shown for the merged, BODIPY TR C5-ceramide, and Rab14-GFP channels plus the positive PDM. The arrows point to Rab14-GFP vesicles outside of the PV, and the arrows with a double arrowhead point to Rab14-GFP vesicles inside the PV. PCC, Pearson *r*.

the vacuole (Figure 10E). The GRASP65 and golgin97 staining within the PV was very faint and showed colocalization with very few Rab14-GFP puncta, which were located more along the edge of the PV. This suggests that the vast majority of intravacuolar Rab14-GFP foci are bona fide Rab vesicles rather than fragments of the host Golgi.

To determine whether Rab14-associated vesicles transport sphingolipids from the TGN to the PV, we analyzed the lipid uptake of infected HeLa cell expressing Rab14-GFP. Infected cells were incubated with BODIPY TR C5-ceramide for 40 min, fixed, and examined by fluorescence microscopy. The fluorescent lipids and GFP-tagged Rab14 signals colocalized in a structure surrounding the PV, which most likely was the host Golgi associated with the PV (Figure 10F). Of more interest, several Rab14-GFP foci that colocalized with red fluorescent puncta were clearly visible inside the PV (Figure 10F). These results suggest that host ceramide is delivered to the PV via Rab14-associated vesicles.

To validate the concept that the parasite intercepts host Golgi–derived vesicles to acquire sphingolipids, we examined the contribution of Rab30-associated vesicles to this process. Rab30-associated vesicles may be a target for *T. gondii* because Rab30 is associated with many compartments of the Golgi complex and is involved in both the maintenance of Golgi structure and vesicular trafficking (de Leeuw *et al.*, 1998; Sinka *et al.*, 2008; Thomas *et al.*, 2009; Kelly *et al.*, 2011). In uninfected cells expressing Rab30-GFP, the fluorescence signal was detected on the Golgi as expected (Figure 11A). In infected cells, Rab30-GFP localized to the host Golgi, which encompassed the PV, as well as to puncta that were observed around and within the PV, where they predominantly accumulated in the center of the vacuole (Figure 11B). We next determined whether any of the Rab30-GFP foci colocalized with GRASP65 and golgin97. As observed for Rab14-GFP, the *cis*-Golgi and TGN markers colocalized with Rab30-GFP on the Golgi, which surrounded the PV (Figure 11, C and D). Very few Rab30-GFP foci within the PV colocalized with either GRASP65 or golgin97 (Figure 11, C and D). To determine whether any of these Rab30-GFP foci were a source of sphingolipids for the parasite, we incubated infected cells expressing Rab30-GFP with BODIPY TR C5-ceramide and analyzed the colocalization of these fluorescently labeled lipids with Rab30-GFP foci. We observed the colocalization of the GFP and red fluorescence signals in the Golgi surrounding the PV and in puncta located within the PV lumen (Figure 11E).

Finally, to confirm our data concerning the ability of the parasite to salvage sphingolipids from Golgi-derived vesicles, we followed the fate of Rab43-GFP in infected cells. Rab43 is located in the *cis*-Golgi, where it colocalizes with GM130, and is involved in anterograde trafficking, most likely from the ER to the Golgi (Dejgaard *et al.*, 2008). In both uninfected and *T. gondii*–infected cells, Rab43-GFP was observed on the Golgi, where it colocalized with both *cis*-Golgi and TGN markers (Supplemental Figure S5, A and B). In infected cells, Rab43-GFP was also observed as puncta within the PV. These puncta rarely, if at all, colocalized with GRASP65 (Supplemental Figure S5A) and partially colocalized with golgin97 on the top or edge of the PV (Supplemental Figure S5B). The Rab43-GFP puncta also colocalized with BODIPY TR C5-ceramide, although to a lesser extent than observed for Rab14- and Rab30-derived foci (Supplemental Figure S5C). These results suggest that the parasite is capable of hijacking numerous Golgi-derived vesicles with selectivity, and these vesicles originate from different stacks of the Golgi, for example, *cis*-Golgi (Rab43) and the TGN (Rab14).

Host sphingolipid uptake is decreased in cells expressing dominant-negative Rab14 and Rab43 mutants but not Rab30 mutants

Finally, to verify the contribution of host Rab14, Rab30, and Rab43 to the scavenging of exogenously added ceramides by the parasite, we measured the fluorescence intensity of BODIPY TR C5-ceramide within the PV of infected cells overexpressing the dominant-negative forms of each Rab protein. Rabs are generally considered constitutively active when bound to GTP and inactive when in a GDP-bound state. Mutations within the conserved motif corresponding to phosphate/Mg^{2+} interacting loop 1 (Ser/Thr to Asn) perturb the cycle of nucleotide binding and hydrolysis, thereby interfering with specific membrane transport steps in a dominant manner (Junutula *et al.*, 2004; Dejgaard *et al.*, 2008). We engineered the constructs Rab14-GFP S25N, Rab43-GFP T32N, and Rab30-GFP T23N. As expected, the three dominant-negative mutants localized to the cytosol and Rab14-GFP S25N also associated with Golgi-like structures (Figure 12A).

The BODIPY TR signal in infected control cells expressing GFP was found on the parasite's plasma membrane and PV (Figure 12A). In contrast, in infected cells expressing the dominant-negative Rab14 and Rab43 mutants, the BODIPY TR signal was abnormally concentrated in large foci on and within the PV, with less staining of the parasite's plasma membrane (Figure 12A). In the infected cells expressing these dominant-negative mutants, the fluorescence intensity of BODIPY TR within the PV and on the parasites was significantly less than the intensity in control cells (Figure 12B). In a separate experiment, infected cells expressing the dominant-negative mutant Rab30 T23N were used, and the fluorescence pattern for BODIPY TR within the PV was similar to that of parasites in control cells (Supplemental Figure S6; compare the fluorescence pattern in the parasites from transfected and untransfected cells on the same coverslip in A). There was no statistically significant difference in the mean arbitrary values of fluorescence intensity for BODIPY TR (Supplemental Figure S6B).

Overall these data highlight the ability of *T. gondii* to intercept host Rab vesicular trafficking pathways, at least those mediated by Rab14, Rab30, and Rab43, and to scavenge sphingolipids from Rab14- and Rab43-associated vesicles delivered within the PV.

DISCUSSION

Although *T. gondii* is capable of de novo sphingolipid synthesis (Azzouz *et al.*, 2002; Sonda *et al.*, 2005; Bisanz *et al.*, 2006), our results suggest that exogenous sources of sphingolipids play a role in parasite growth (summarized in Figure 9). For example, exogenously added ceramides that are processed in the Golgi and scavenged from this organelle in a parasite-mediated manner enhance parasite replication. In addition, other host sources of sphingolipids may be beneficial to the parasite because perturbing host sphingolipid metabolism and production in the ER and at the plasma membrane has a negative effect on parasite growth. These effects on the parasite may result not only from the lack of sphingolipids available for incorporation into the parasite's membranes, but also from changes in host cell signaling pathways. Ceramides have pleiotropic signaling properties and have been implicated in diverse cellular processes such as apoptosis, proliferation, and differentiation (Hannun and Obeid, 2008). By diverting sphingolipids from the host cell, the parasite may—purposively or not—affect signaling pathways, which may enhance the parasite's replication or cause changes in the host cell that the parasite must mitigate. Of interest, it has been hypothesized that host ceramide signaling is involved in cyst formation of *T. gondii*, since treatment of cells infected with the cystogenic

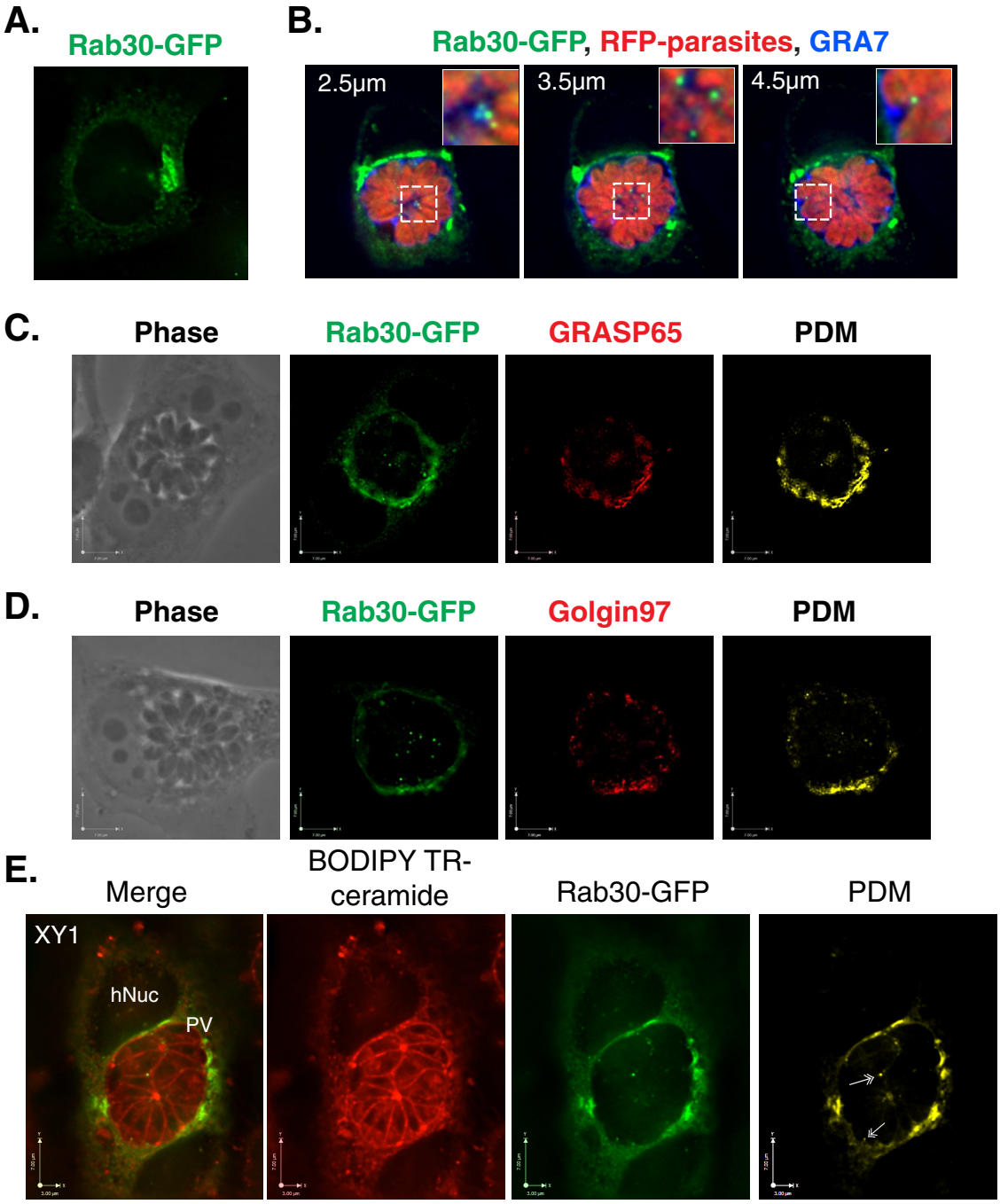

FIGURE 11: Interception of host Rab30 vesicles by *T. gondii*. (A) HeLa cells expressing Rab30-GFP (green) were fixed and viewed by fluorescence microscopy. An individual optical *z*-slice is shown. (B) HeLa cells expressing Rab30-GFP (green) were infected for 30 h with *T. gondii* RH parasites expressing RFP (red), fixed, and stained with antibodies against GRA7 (blue). Optical *z*-slices are shown. The inset is a magnified view of the boxed region. (C) HeLa cells expressing Rab30-GFP (green) were infected for 32 h with *T. gondii* RH, fixed, and stained with antibodies against GRASP65 (red). An optical *z*-slice is shown for the phase, Rab30-GFP, and GRASP65 channels plus the positive PDM. (D) HeLa cells expressing Rab30-GFP (green) were infected for 32 h with *T. gondii* RH, fixed, and stained with antibodies against golgin97 (red). An optical *z*-slice is shown for the phase, Rab30-GFP, and golgin97 channels plus the positive PDM. (E) HeLa cells were transfected with Rab30-GFP (green), infected with RH parasites for 30 h, and incubated in the presence of BODIPY TR C5-ceramide (red) for 40 min. An optical *z*-slice is shown for the merged, BODIPY TR C5-ceramide, and Rab30-GFP channels plus the positive PDM. The double arrowheads point to Rab30-GFP vesicles inside the PV. hNuc, host nucleus; PCC, Pearson *r*.

Prugniaud strain with the inhibitor tricyclodecan-9-yl-xanthogenate resulted in a decreased production of cysts (Ricard *et al.*, 1996). Although changes in host sphingolipid metabolism affect parasite growth, the respective contribution of host- and parasite-derived sphingolipids to support parasite growth remains to be determined. The parasite, however, appears to have developed redundant

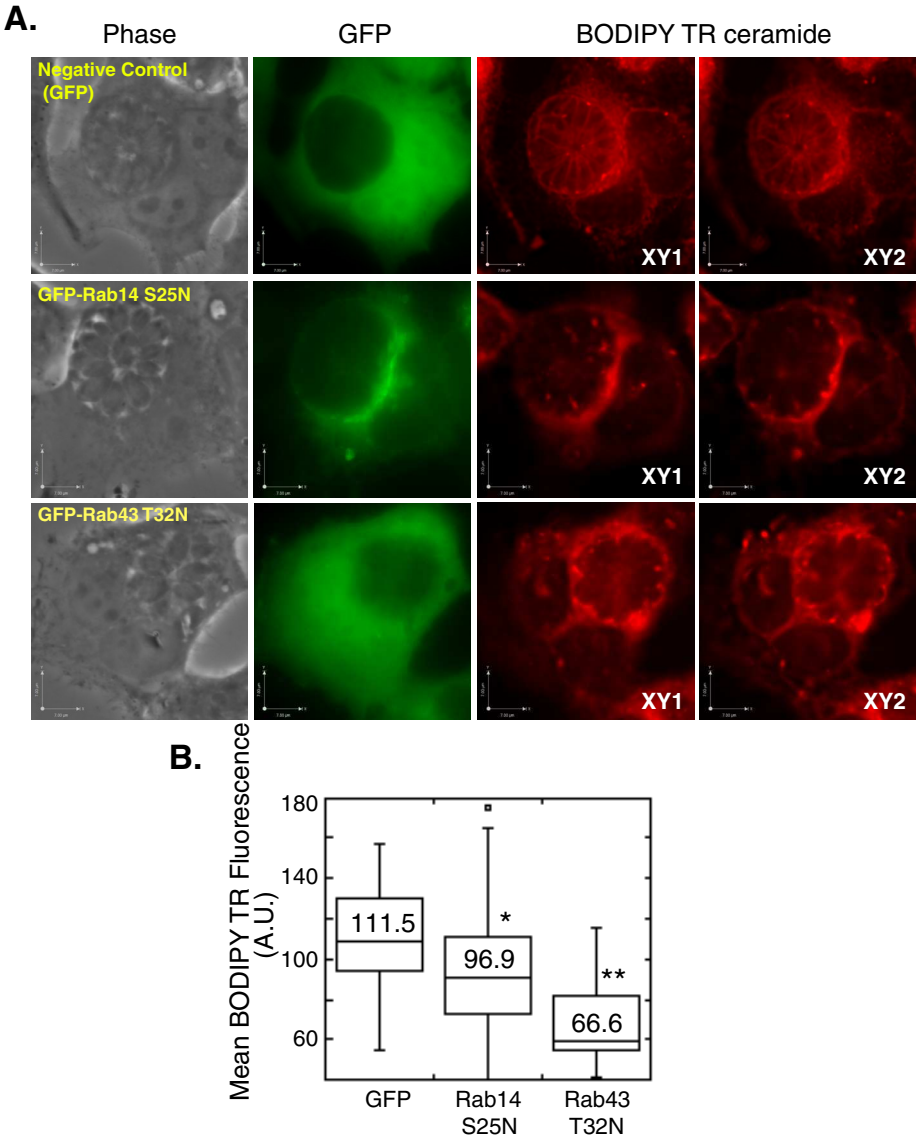

FIGURE 12: Effect of dominant-negative Rab14 and Rab43 mutants on BODIPY TR C5-ceramide staining of the PV. HeLa cells were transfected with GFP (negative control), GFP-Rab14 S25N, or GFP-Rab43 T32N, infected with *T. gondii* RH for 32 h, and incubated with BODIPY TR C5-ceramide for 60 min. (A) Phase and GFP images, as well as two optical *z*-slices of the BODIPY TR channel, for HeLa cells transfected with GFP, GFP-Rab14 S25N, and GFP-Rab43 T32N. Scale bars, 7 μm for *x*- and *y*-axes. (B) Box plot showing the distribution of mean BODIPY TR fluorescence intensity values within the PV of infected cells expressing the negative control GFP or the dominant-negative mutants of GFP-Rab14 S25N or GFP-Rab43 T32N. Whiskers of the box plots represent upper and lower values excluding outliers, outliers are marked as open circles, and the line inside the box is the median value. The numbers written within the plot are the mean fluorescence intensities. Mean fluorescence intensity was measured for 34, 35, and 27 PVs for GFP control, GFP-Rab14 S25N, and GFP-Rab43 T32N, respectively. *$p < 0.05$, **$p < 0.001$.

salvage pathways to acquire host sphingolipids, which suggests that the contribution of host sources of these lipids may be significant for parasite growth.

The active scavenging of sphingolipids from the host Golgi by *T. gondii* emphasizes the importance of this Golgi–PV interaction for the parasite. We propose the following model. The parasite 1) associates closely with the host Golgi and localizes near the MTOC, 2) destabilizes the structure of the Golgi, resulting in its breakdown into ministacks, which encircle the PV, 3) intercepts Golgi-derived vesicles, 4) sequesters Rab14-, Rab30-, or Rab43-associated vesicles containing sphingolipids within the PV, and 5) incorporates sphingolipids into its plasma membrane and internal organelles. During an infection, the PV associates not only with the host Golgi, but also with the MTOC. The role of the MTOC in organizing the microtubule network of cells and in positioning the Golgi suggests that the PV may associate with this host structure to use host microtubules to enable its association with host organelles. In fact, host microtubules have been shown to encompass the PV (Melo *et al.*, 2001; Coppens *et al.*, 2006 ; Walker *et al.*, 2008). Our results suggest, however, that the PV–MTOC association is not a prerequisite for the attraction of the Golgi by the PV, as we observed a PV–Golgi association before recruitment of the host MTOC. In accordance with these results, the loss of PV–MTOC association in cells with defects in the mTORC2-Akt pathway led to changes in the distribution of host mitochondria and lysosomes to the PV but not in the association of these organelles with the PV (Wang *et al.*, 2010). Thus the MTOC may not play a role in the initial interaction of the PV with host organelles but may be involved in the organization and maintenance of these organelles around the PV, possibly through its arrangement of host microtubules, which surround the PV (Melo *et al.*, 2001; Coppens *et al.*, 2006; Walker *et al.*, 2008).

During a *T. gondii* infection, the host Golgi is fragmented into ministacks, which remain closely associated with the PV. The destabilization of the Golgi structure may aid the parasite in scavenging lipids by facilitating the acquisition of Golgi-derived vesicles. In fact, the Golgi is fragmented into ministacks during an infection with *C. trachomatis*, and this event enhances bacterial replication (Heuer *et al.*, 2009). Astonishingly, in a *T. gondii* or *C. trachomatis* infection, the morphology of the host Golgi is very similar, as in both cases the Golgi fragments resemble shortened structures as if the Golgi had been sliced into ministacks. The maintenance of the stacked cisternae morphology of the Golgi during the infection may imply the continued functionality of this organelle, allowing the pathogens to rely on its synthetic activities. In the case of a *C. trachomatis* infection, host golgin84 is cleaved, leading to the destabilization of the Golgi structure (Heuer *et al.*, 2009). A secreted protease of bacterial origin has been proposed to be involved in the cleavage of host golgin84, but the identity of the protease is controversial (Christian *et al.*, 2011; Chen *et al.*, 2012). Our results suggest that *T. gondii* mediates a process of Golgi fragmentation different from that of *C. trachomatis*, as no cleavage of host golgins was detected during an infection.

Alternatively, the dismantling and dispersion of the Golgi in *Toxoplasma*-infected cells may be related to the interception of host Golgi–derived Rab vesicles, followed by the trapping of these vesicles in the PV lumen. Indeed, the structure of the Golgi is very sensitive to perturbations in vesicular trafficking. For instance, the microinjection of mutant Rab1a proteins defective in GTPase hydrolysis resulted in the breakdown of the Golgi into dispersed vesicular structures (Wilson *et al.*, 1994).

Intercepting host Rab GTPases is a tactic shared by a number of different intracellular pathogens. For example, *Mycobacterium* sp., *Salmonella enterica* serovar Typhimurium, *Anaplasma phagocytophilium*, and *Legionella pneumophila* regulate the biogenesis of their phagosome by selectively excluding and/or retaining specific host Rab proteins (Via *et al.*, 1997; Méresse *et al.*, 1999; Machner and Isberg, 2006; Murata *et al.*, 2006; Huang *et al.*, 2010). Given that *T. gondii* bypasses the host cell's phagocytic machinery by actively invading cells and forming its own PV, this is not a strategy shared by the parasite; the parasite does not need to incorporate host Rab GTPases (or any host proteins) into the PV membrane to modify its vacuole. Instead *T. gondii* hijacks host endocytic and exocytic trafficking vesicles for their lipid cargoes, as *C. trachomatis* does (Rzomp *et al.*, 2003; Capmany and Damiani, 2010). For example, the *T. gondii* PV redirects host endocytic compartments containing cholesterol-LDL (Coppens *et al.*, 2006) and reroutes sphingolipid-containing Golgi-derived vesicles, which are marked with Rab14, Rab30, or Rab43, to the PV lumen.

The presence of host-derived vesicles within the lumen of the *T. gondii* PV suggests that these vesicles can cross the PVM as intact structures. In a previous study, we described a process termed "host organelle–sequestering tubule structures" by which host microtubules push into the PVM, forming large invaginations that serve as conduits for the uptake of host endocytic vesicles (Coppens *et al.*, 2006). The PVM not only forms these invaginations, but it has the ability to form PVM projections (evaginations) that extend throughout the host cytosol (Coppens *et al.*, 2006; Rome *et al.*, 2008), demonstrating the dynamic nature of this membrane. The high deformability of the PVM is a characteristic shared with the plasma membrane from which it was derived. Thus it is tempting to propose that the PVM functions as a plasma membrane endowed with the capacity to "phagocytose" large structures, such as host vesicles, present near the PV. In fact, we showed that host endosomes containing gold-labeled LDL particles are taken up into the PV lumen as intact vesicles. These host vesicles are enclosed by the PV membrane, suggesting that the PV may be able to "phagocytose" host endosomes (Coppens *et al.*, 2006). We can envisage a similar scenario for the host Golgi–derived vesicles that are trapped into the vacuolar space and may also be surrounded by the PVM. The presence of pores within the PVM for the transit of small nutrients from the host cytosol (Schwab *et al.*, 1994) and the trapping of host organelles loaded in lipids into the PV, coupled with the secretion of parasite enzymes involved in the processing of nutrients in the vacuole (Sibley *et al.*, 1994), strongly suggest that the PV lumen may function as a large extracellular digestive compartment for the parasite.

Our results pinpoint a general mechanism for lipid scavenging by *T. gondii* that involves the uptake of host vesicles and their associated material into the PV lumen. In this way, the parasite acquires the needed nutrients by circumventing fusion with host organelles.

MATERIALS AND METHODS

Reagents and antibodies

All reagents were purchased from Sigma-Aldrich (St. Louis, MO), unless otherwise stated. NBD C6-ceramide and BODIPY C5-ceramide, both complexed to bovine serum albumin (BSA), were obtained from Molecular Probes (Seattle, WA) and Invitrogen (Carlsbad, CA), respectively. Lipid standards (ceramide and sphingomyelin) for TLC were from Matreya LLC (Pleasant Gap, PA). The following primary antibodies were used: mouse monoclonal and rabbit polyclonal anti-γ-tubulin; rabbit polyclonal anti-GRASP65 (Novus Biologicals, Littleton, CO); rabbit polyclonal anti-giantin and anti-pericentrin (Covance, Emeryville, CA); mouse monoclonal anti-golgin97 (Invitrogen); rabbit polyclonal anti-golgin160 (a generous gift from Carolyn Machamer, Johns Hopkins University School of Medicine, Baltimore, MD); rabbit polyclonal or rat monoclonal anti-GRA7 antibodies (Coppens *et al.*, 2006); and mouse monoclonal anti-Hsp70 antibodies (generously provided by Fidel Zavala, Johns Hopkins University Bloomberg School of Public Health). Secondary antibodies used for immunofluorescence were conjugated to Alexa 488, Alexa 594, or Alexa 350 (Invitrogen).

Cell culture and transfection

VERO cells, HeLa cells, HFFs, and CHO-K1 were obtained from the American Type Culture Collection (Manassas, VA). The LY-B cell line was obtained from the RIKEN Bio Resource Center (Ibaraki, Japan). NHF and NPD-A were obtained from the Mental Retardation Research Center (Kennedy Krieger Institute, Baltimore, MD). MDCK cells were generously provided by Andrew Pekosz (Johns Hopkins University Bloomberg School of Public Health). The human HepG2 cell line stably transfected with CD81 (HepG2-CD81) was kindly provided by D. Mazier (Université Pierre et Marie Curie, Paris, France). All cell lines were maintained at 37°C in an atmosphere of 5% CO_2. Except for LY-B and CHO-K1, the cells were grown in Alpha MEM (Corning Cellgro, Manassas, VA) supplemented with 10% (vol/vol) fetal bovine serum, 2 mM L-glutamine, and penicillin/streptomycin (100 U/ml per 100 µg/ml). The LY-B and CHO-K1 cell lines were maintained in Ham's F12 medium supplemented with 10% newborn calf serum (Life Technologies, Paisly, United Kingdom), 1 mM L-glutamine, 100 U/ml penicillin, and 100 mg/ml streptomycin (Life Technologies). To reduce the cellular sphingolipid level in the LY-B cell line, the cells were seeded out in NBO medium on polylysine-coated Falcon culture plates (BD, Franklin Lakes, NJ) 2 d before experiments. The NBO medium is based on Ham's F12 medium supplemented with 0.1% fetal calf serum, 1% Nutridoma-SP (Roche Diagnostics, Mannheim, Germany), 10 mM sodium oleate complexed with fatty acid–free BSA, 100 U/ml penicillin, and 100 mg/ml streptomycin.

HeLa cells were used for all transfections and were transfected using 2 µg of plasmid DNA and the Amaxa Nucleofector solution R according to the manufacturer's instructions (Lonza, Basel, Switzerland). HeLa cells were also used in immunofluorescence assays with the anti-golgin97 antibody, since the antibody is specific for human golgin97.

Plasmids

The NEDD1-GFP plasmid was a generous gift from Andreas Merdes (Institut de Sciences et Technologies du Médicament de Toulouse, Center National de la Recherche Scientifique, Toulouse, France). The GFP-Rab14, GFP-Rab30, and GFP-Rab43 constructs were kindly

provided by John Presley (McGill University, Montreal, Canada). The dominant-negative mutants GFP-Rab30 T23N and GFP-Rab43 T32N were created by site-directed mutagenesis of the corresponding wild-type plasmids using forward primers 5′-GGAAGAACTGCCTCGTCCGAAGATTCACTCAGGG-3′and5′-GGGCAAGAACTGCGTGGTGCAGCGCTTCAAG-3′ and reverse primers 5′-TTCGGACGAGGCAGTTCTTCCCCACACCAGCGTTG-3′ and 5-ACCACGCAGTTCTTGCCCACGCTTGCGTCGC-3′, respectively. The dominant-negative mutant GFP-Rab14 S25N was created by PCR in two steps. First, GFP-Rab14 was amplified, in two separate PCRs, using the following pairs of primers: 1) forward primer 5′-CACCAAAATCAACGGGACTT-3′ and reverse primer with the mutation 5′-GGGGACATGGGAGTAGGAAAAAATTGCTTGCTTCATCAATTTAC-3′ and 2) forward primer with the mutation 5′-GTAAATTGATGAAGCAAGCAATTTTTTCCTACTCCCATGTCCCC-3′ and reverse primer 5′-GGGAGGTGTGGGAGGTTTT-3′. Second, the PCR products were combined using the forward and reverse primers 5′-CACCAAAATCAACGGGACTT-3′ and 5′-GGGAGGTGTGGGAGGTTTT-3′, respectively. The mutant was subcloned into the pEGFP vector (Clontech, Mountain View, CA) using *Nhe*I and *Bam*HI. All sequences were confirmed by DNA sequencing.

Pathogen strains and infection conditions

The tachyzoite RH strain of *T. gondii* was used throughout this study. The RH strain stably expressing RFP was generously provided by Florence Dzierszinski (McGill University, Montreal, Canada). In one set of experiments, the cystogenic strain Prugniaud (generously provided by David Roos, University of Pennsylvania, Philadelphia, PA) was used. The parasites were propagated in vitro by serial passage in monolayers of HFF cells (Roos *et al*., 1994). The *P. yoelii* strain XNL was grown in *Anopheles stephensi* mosquitoes blood fed on infected Swiss CD-1/ICR mice as described (Kaiser *et al*., 2003). Seeds of the *C. trachomatis* lab reference serovar E/UW5-CX were generously provided by Patrik Bavoil (University of Maryland Dental School, Baltimore, MD).

Unless otherwise stated, VERO or HeLa cells were grown to ~70% confluence and infected with *T. gondii* parasites for 30 min at 37°C, washed with phosphate-buffered saline (PBS) to remove extracellular parasites, and incubated at 37°C for the times indicated. MDCK cells were grown on coverslips for 10 d at 37°C before infection with *T. gondii* parasites.

Plaque assay

HFF cells were grown until confluent in a six-well plate. Two hundred parasites were added per well, and the plates were incubated at 37°C for 7 d. The cells were fixed and stained as described previously (Striepen and Soldati-Favre, 2007). The plates were scanned (ScanWizard 5; Microtek, Santa Fe Springs, CA), and the area of each plaque was measured using Volocity software (PerkinElmer, Waltham, MA) by tracing each plaque using the ROI tool. The mean area and SD of the plaques were calculated from three independent experiments, and the *p* value was calculated using a Student's *t* test with Excel software (Microsoft, Redmond, WA).

Uracil incorporation assay

HFF cells were grown until confluent in 24-well plates. HFF cells were infected with 1×10^5 parasites for 4 h at 37°C, washed twice with PBS, and incubated for 24 h in Alpha MEM. Cells were incubated with 1 μCi of [^{3}H]uracil (PerkinElmer, Shelton, CT) for 2 h at 37°C, and the samples were processed as described previously (Pfefferkorn and Guyre, 1984; Roos *et al*., 1994).

Lipid analyses

Ceramide uptake. To monitor the uptake of ceramides by intravacuolar *Toxoplasma* (RH or Prugniaud strains), HFFs were infected for 24 h, washed with PBS, and incubated in serum-free medium containing 5 μM NBD C6-ceramide complexed to BSA for different times before observations by live fluorescence microscopy.

Ceramide isolation. To assess ceramide incorporation into major sphingolipids by *Toxoplasma*, HFFs were infected for 24 h at multiplicity of infection (MOI) of 10 and incubated with 5 μM NBD C6-ceramide-BSA in serum-free medium for 1 or 6 h. Parasites were then forced to egress by addition of the calcium ionophore A23187 as described (Endo *et al*., 1982), collected in the supernatant, and purified from host cell contaminants as described (Coppens *et al*., 2000). Total lipids from parasites were extracted with chlorofom:methanol:water (10:10:3, vol/vol/vol), dried under liquid N_2, and subjected to *n*-butanol/water partitioning. Lipids recovered from the butanol phase were fractionated by TLC in chloroform:methanol:ammonium hydroxide (65:25:4, vol/vol/vol) on TLC Silica Gel 60 plates (Merck, Gibbsburg, NJ). NBD fluorescent lipids were visualized with a FLA-5000 fluorescence image analyzer equipped with FLA-5000 image reader software (Fujifilm, Tokyo, Japan).

Immunofluorescence and cell staining

Cells were fixed with either 4% formaldehyde (Polysciences, Warrington, PA) plus 0.02% glutaraldehyde (Sigma-Aldrich) in PBS for 15 min or in cold 100% methanol for 5 min (for immunostaining with γ-tubulin or pericentrin antibodies). Immunofluorescence assays were performed as described previously (Karsten *et al*., 2004), except that the permeabilization step with 0.3% Triton X-100 in PBS was omitted for samples fixed with methanol. Coverslips were mounted using ProLong antifade mounting solution (Invitrogen).

HeLa cells were transfected with Rab14-GFP, Rab30-GFP, or Rab43-GFP and allowed to recover overnight at 37°C. The cells were infected with RH parasites for 45 min at 37°C, washed with PBS to remove extracellular parasites, and incubated for 30 h at 37°C. The cells were incubated with serum-free medium containing 5 μM BODIPY C5-ceramide conjugated to BSA for 40 or 60 min. The samples were washed with PBS and fixed with 4% paraformaldehyde (EM grade; Electron Microscopy Sciences, Hatfield, PA) and 0.02% glutaraldehyde (EM grade) in PBS for 20 min. Samples were then washed with PBS and mounted using ProLong antifade mounting solution (Invitrogen).

Fluorescence microscopy

Live cells were viewed on a Nikon Eclipse E800 microscope (Nikon, Melville, NY) equipped with an oil-immersion plan Apo 100×/numerical aperture (NA) 1.4 objective. Images were acquired with a Spot RT charge-coupled device camera (Diagnostic Instruments, Sterling Heights, MI) and Image-Pro-Plus software (Media Cybernetics, Silver Spring, MD). Photoshop (Adobe, San Jose, CA) was used to adjust levels and crop and resize images.

Fixed samples were viewed with a fluorescence microscope (Nikon Eclipse 90i) equipped with an oil-immersion plan Apo 100×/NA 1.4 objective and a Hamamatsu GRCA-ER camera (Hamamatsu Photonics, Hamamatsu, Japan). For the experiment involving the dominant-negative mutant Rab30 T23N, the oil-immersion plan Apo 60×/NA 1.4 objective was used. Optical *z*-sections with 0.2-μm spacing were acquired using Volocity software. The images were deconvolved using an iterative restoration algorithm, and the

registry was corrected using Volocity software. Photoshop was used to adjust levels and crop and resize images.

The shortest distance between the PV and the host MTOC (represented by γ-tubulin foci and pericentrin foci) was measured using Volocity software on a 3D reconstructed volume and displayed in a box plot. Likewise, the distance between the PV and the closest part of the host Golgi, as detected with antibodies against giantin, was measured and displayed in a box plot. Outliers were calculated to be either greater than the upper quartile plus 1.5 times the interquartile distance or less than the lower quartile minus 1.5 times the interquartile distance. The upper and lower quartiles are the values halfway between the median and the largest or smallest data value, respectively. The interquartile distance is the distance between the upper and lower quartiles. No outliers were excluded from calculations of mean distance or *p* values.

The number and volume of giantin foci present in uninfected and *T. gondii*–infected cells were measured on 3D reconstructed volumes using Volocity software, where individual giantin foci were identified by intensity using automatic thresholding, and objects $<0.2\ \mu m^3$ were excluded from the calculations. The mean volume and SD were calculated from three independent experiments using Excel.

To compare the amount of BODIPY TR signal in the PVs of HeLa cells expressing the dominant-negative Rab mutants or the vector control, we analyzed the fluorescence intensity of the BODIPY TR signal on images captured using the same exposure time and gain and offset values. To do so, we sampled several regions within each PV using a region of interest of fixed size. The mean intensity of the fluorescence signal was calculated and subtracted from the mean background fluorescence intensity. The mean background intensity was determined by measuring the fluorescence intensity using a region of interest of fixed size of four regions located between cells on the slides. The data are displayed in a box plot generated as described. No outliers were excluded from calculations of mean fluorescence intensity or *p* values.

Pearson *r* and the positive PDM images were calculated using Volocity software. Thresholds were set automatically using the method of Costes (Costes *et al.*, 2004).

To measure the number of parasites within a PV after 24 h of infection with either RH or Prugniaud strains, the samples were viewed with phase-contrast microscopy, and the number of parasites within a vacuole was counted. The mean number of parasites and SD was calculated from three independent experiments using Excel.

HeLa cells infected with either RH or Prugniaud parasites for 24 h were grouped into three categories (around, close, and far) based on the level of association between the host Golgi and the PV. The "around" category included PVs that were surrounded by the host Golgi, and the "close" category included PVs in which the host Golgi touched the PV without surrounding it. The "far" category included PVs that were distant from the host Golgi. The percentage of PVs that fell into each category was determined, and the mean percentage and SD were calculated from three independent experiments using Excel.

Transmission electron microscopy

For ultrastructural observations of the host Golgi in cells infected with *T. gondii* by thin-section transmission electron microscopy, infected VERO cells were fixed 24 or 48 h p.i. in 2.5% glutaraldehyde (Electron Microscopy Sciences) and processed as described (Coppens and Joiner, 2003). Ultrathin sections of infected cells were stained before examination with a Philips CM120 EM (Eindhoven, Netherlands) under 80 kV. Quantification of Golgi fragments from the EM images was performed by determining the number and size of Golgi elements in 25 cells per infection time (on infected and uninfected cells at 24 and 48 h) using sequential random sampling protocols for morphometrical analyses (Mayhew and Gundersen, 1996). For immuno–electron microscopy of the host Golgi, *Toxoplasma*-infected HFFs were fixed in 4% paraformaldehyde 24 h p.i. (Electron Microscopy Sciences) and processed as previously described (Quittnat *et al.*, 2004). The sections were immunolabeled with anti-giantin antibodies (1/5 in PBS/1% fish skin gelatin) and then with goat anti-rabbit immunoglobulin G antibodies, followed directly by 10 nm of protein A–gold particles (Department of Cell Biology, Medical School, Utrecht University, Netherlands) before microscopic examination.

Cell lysates and immunoblotting

HeLa cells were infected at 37°C with *T. gondii* RH parasites for 30 h with MOI of 2. To prepare *C. trachomatis*, a frozen stock of bacterial seeds was sonicated at 37°C, and SPG buffer (0.25 M sucrose, 10 mM sodium phosphate, and 5 mM L-glutamic acid) was added to the bacteria. Then the bacteria were added to HeLa cells grown in Alpha MEM without antibiotics but containing 10% fetal bovine serum and 2 mM L-glutamine. The flask was centrifuged at room temperature for 30 min and then incubated at 37°C for 30 min. The SPG buffer was removed, and the cells were incubated in medium without antibiotics for 30 h at 37°C. Cell lysates from uninfected, *T. gondii*–infected, and *C. trachomatis*–infected HeLa cells were prepared according to the manufacturer's instructions, using the mammalian protein extraction reagent M-Per (Thermo Scientific, Rockford, IL) plus 0.5 mM phenylmethylsulfonyl fluoride, 20 µM leupeptin, 40 µM bestatin, 15 µM pepstatin A, 14 µM E-64, 0.8 µM aprotinin, and 1 µM 4-(2-aminoethyl) benzenesulfonyl fluoride hydrochloride. The protein concentration of each lysate was determined using a Micro BCA protein assay (Thermo Scientific) according to the manufacturer's instructions. Proteins were precipitated with 5.5% trichloroacetic acid on ice for 30 min, resuspended in SDS gel loading buffer (63 mM Tris-Cl, pH 6.8, 2.3% SDS, 10% glycerol, 5% 2-mercaptoethanol, 0.01% bromophenol blue), and boiled. Cell lysates (50 µg proteins) were separated by SDS–PAGE and transferred to a polyvinylidene fluoride membrane (Millipore, Bedford, MA). The membrane was probed as described previously (Lige *et al.*, 2011) using either rabbit anti-golgin160 (1:5000) or mouse anti-golgin97 (1:5000) antibodies and detected by chemiluminescence.

Statistical methods

Data are displayed in box plots using Kaleidagraph software (Synergy Software, Reading, PA). Whiskers of the box plots represent the upper and lower values excluding outliers, outliers are marked as open circles, and the line inside the box is the median value. Means and SDs are calculated from three independent experiments using Excel. The *p* values were calculated using either Student's *t* test in Excel or from a one-way analysis of variance with a post hoc Bonferroni test in Kaleidagraph.

ACKNOWLEDGMENTS

We thank the members of the Coppens laboratory for helpful discussions during the course of this work and the technical staff of the Yale Microscopy Facility (New Haven, CT). We acknowledge Carolyn Machamer for helpful advice in the Golgi analyses and excellent critical reading of the manuscript. We also thank Jose Carrasco (University of Maryland, Baltimore, MD) for providing the seeds of *Chlamydia*. This work was supported by National Institutes of Health Grant AI060767 to I.C.

REFERENCES

Azzouz N, Rauscher B, Gerold P, Cesbron-Delauw M-F, Dubremetz J-F, Schwarz RT (2002). Evidence for de novo sphingolipid biosynthesis in *Toxoplasma gondii*. Int J Parasitol 32, 677–684.

Bacallao R, Antony C, Dotti C, Karsenti E, Stelzer EH, Simons K (1989). The subcellular organization of Madin-Darby canine kidney cells during the formation of a polarized epithelium. J Cell Biol 109, 2817–2832.

Barr FA, Short B (2003). Golgins in the structure and dynamics of the Golgi apparatus. Curr Opin Cell Biol 15, 405–413.

Bisanz C, Bastien O, Grando D, Jouhet J, Maréchal E, Cesbron-Delauw M-F (2006). *Toxoplasma gondii* acyl-lipid metabolism: de novo synthesis from apicoplast-generated fatty acids versus scavenging of host cell precursors. Biochem J 394, 197–205.

Breslow DK, Weissman JS (2010). Membranes in balance: mechanisms of sphingolipid homeostasis. Mol Cell 40, 267–279.

Capmany A, Damiani MT (2010). *Chlamydia trachomatis* intercepts Golgi-derived sphingolipids through a rab14-mediated transport required for bacterial development and replication. PLoS One 5, e14084.

Cesbron-Delauw M-F, Gendrin C, Travier L, Ruffiot P, Mercier C (2008). Apicomplexa in mammalian cells: trafficking to the parasitophorous vacuole. Traffic 9, 657–664.

Charron AJ, Sibley LD (2004). Molecular partitioning during host cell penetration by *Toxoplasma gondii*. Traffic 5, 855–867.

Chen AL, Johnson KA, Lee JK, Sütterlin C, Tan M (2012). CPAF: a chlamydial protease in search of an authentic substrate. PLoS Pathog 8, e1002842.

Chiu R, Novikov L, Mukherjee S, Shields D (2002). A caspase cleavage fragment of p115 induces fragmentation of the Golgi apparatus and apoptosis. J Cell Biol 159, 637–648.

Christian JG, Heymann J, Paschen SA, Vier J, Schauenburg L, Rupp J, Meyer TF, Häcker G, Heuer D (2011). Targeting of a chlamydial protease impedes intracellular bacterial growth. PLoS Pathog 7, e1002283.

Coppens I (2006). Contribution of host lipids to *Toxoplasma* pathogenesis. Cell Microbiol 8, 1–9.

Coppens I, Dunn JD, Romano JD, Pypaert M, Zhang H, Boothroyd JC, Joiner KA (2006). *Toxoplasma gondii* sequesters lysosomes from mammalian hosts in the vacuolar space. Cell 125, 261–274.

Coppens I, Joiner KA (2003). Host but not parasite cholesterol controls *Toxoplasma* cell entry by modulating organelle discharge. Mol Biol Cell 14, 3804–3820.

Coppens I, Sinai AP, Joiner KA (2000). *Toxoplasma gondii* exploits host low-density lipoprotein receptor-mediated endocytosis for cholesterol acquisition. J Cell Biol 149, 167–180.

Costes SV, Daelemans D, Cho EH, Dobbin Z, Pavlakis G, Lockett S (2004). Automatic and quantitative measurement of protein-protein colocalization in live cells. Biophys J 86, 3993–4003.

de Leeuw HP, Koster PM, Calafat J, Janssen H, van Zonneveld AJ, van Mourik JA, Voorberg J (1998). Small GTP-binding proteins in human endothelial cells. Br J Haematol 103, 15–19.

de Melo EJ, De Souza W (1996). Pathway of C6-NBD-Ceramide on the host cell infected with *Toxoplasma gondii*. Cell Struct Funct 21, 47–52.

Dejgaard SY *et al*. (2008). Rab18 and Rab43 have key roles in ER-Golgi trafficking. J Cell Sci 121, 2768–2781.

Dobrowolski JM, Sibley LD (1996). *Toxoplasma* invasion of mammalian cells is powered by the actin cytoskeleton of the parasite. Cell 84, 933–939.

Dubey J (1977). *Toxoplasma*, *Hammondia*, *Besnoitia*, *Sarcocystis*, and other tissue cyst-forming coccidia of man and animals. In: Parasitic Protozoa, ed. JP Kreier, New York: Academic Press, 101–237.

Ehrenman K, Sehgal A, Lige B, Stedman TT, Joiner KA, Coppens I (2010). Novel roles for ATP-binding cassette G transporters in lipid redistribution in *Toxoplasma*. Mol Microbiol 76, 1232–1249.

Endo T, Sethi KK, Piekarski G (1982). *Toxoplasma gondii*: calcium ionophore A23187-mediated exit of trophozoites from infected murine macrophages. Exp Parasitol 53, 179–188.

Hanada K, Hara T, Fukasawa M, Yamaji A, Umeda M, Nishijima M (1998). Mammalian cell mutants resistant to a sphingomyelin-directed cytolysin. Genetic and biochemical evidence for complex formation of the LCB1 protein with the LCB2 protein for serine palmitoyltransferase. J Biol Chem 273, 33787–33794.

Hannun YA, Obeid LM (2008). Principles of bioactive lipid signalling: lessons from sphingolipids. Nat Rev Mol Cell Biol 9, 139–150.

Heuer D, Rejman Lipinski A, Machuy N, Karlas A, Wehrens A, Siedler F, Brinkmann V, Meyer TF (2009). *Chlamydia* causes fragmentation of the Golgi compartment to ensure reproduction. Nature 457, 731–735.

Huang B, Hubber A, McDonough JA, Roy CR, Scidmore MA, Carlyon JA (2010). The *Anaplasma phagocytophilum*-occupied vacuole selectively recruits Rab-GTPases that are predominantly associated with recycling endosomes. Cell Microbiol 12, 1292–1307.

Junutula JR, De Maziére AM, Peden AA, Ervin KE, Advani RJ, van Dijk SM, Klumperman J, Scheller RH (2004). Rab14 is involved in membrane trafficking between the Golgi complex and endosomes. Mol Biol Cell 15, 2218–2229.

Kaiser K, Camargo N, Kappe SHI (2003). Transformation of sporozoites into early exoerythrocytic malaria parasites does not require host cells. J Exp Med 197, 1045–1050.

Karsten V, Hegde RS, Sinai AP, Yang M, Joiner KA (2004). Transmembrane domain modulates sorting of membrane proteins in *Toxoplasma gondii*. J Biol Chem 279, 26052–26057.

Kelly EE, Giordano F, Horgan CP, Jollivet F, Raposo G, McCaffrey MW (2011). Rab30 is required for the morphological integrity of the Golgi apparatus. Biol Cell 104, 84–101.

Kitt KN, Hernández-Deviez D, Ballantyne SD, Spiliotis ET, Casanova JE, Wilson JM (2008). Rab14 regulates apical targeting in polarized epithelial cells. Traffic 9, 1218–1231.

Kupfer A, Louvard D, Singer SJ (1982). Polarization of the Golgi apparatus and the microtubule-organizing center in cultured fibroblasts at the edge of an experimental wound. Proc Natl Acad Sci USA 79, 2603–2607.

Lane JD, Lucocq J, Pryde J, Barr FA, Woodman PG, Allan VJ, Lowe M (2002). Caspase-mediated cleavage of the stacking protein GRASP65 is required for Golgi fragmentation during apoptosis. J Cell Biol 156, 495–509.

Lige B, Romano JD, Bandaru VVR, Ehrenman K, Levitskaya J, Sampels V, Haughey NJ, Coppens I (2011). Deficiency of a Niemann-Pick, type C1-related protein in *Toxoplasma* is associated with multiple lipidoses and increased pathogenicity. PLoS Pathog 7, e1002410.

Lipsky NG, Pagano RE (1985). Intracellular translocation of fluorescent sphingolipids in cultured fibroblasts: endogenously synthesized sphingomyelin and glucocerebroside analogues pass through the Golgi apparatus en route to the plasma membrane. J Cell Biol 100, 27–34.

Lowe M, Lane JD, Woodman PG, Allan VJ (2004). Caspase-mediated cleavage of syntaxin 5 and giantin accompanies inhibition of secretory traffic during apoptosis. J Cell Sci 117, 1139–1150.

Luft BJ, Remington JS (1992). Toxoplasmic encephalitis in AIDS. Clin Infect Dis 15, 211–222.

Machner MP, Isberg RR (2006). Targeting of host Rab GTPase function by the intravacuolar pathogen *Legionella pneumophila*. Dev Cell 11, 47–56.

Mancini M, Machamer CE, Roy S, Nicholson DW, Thornberry NA, Casciola-Rosen LA, Rosen A (2000). Caspase-2 is localized at the Golgi complex and cleaves golgin-160 during apoptosis. J Cell Biol 149, 603–612.

Mayhew TM, Gundersen HJ (1996). "If you assume, you can make an ass out of u and me": a decade of the disector for stereological counting of particles in 3D space. J Anat 188, 1–15.

Melo EJ, Carvalho TM, De Souza W (2001). Behaviour of microtubules in cells infected with *Toxoplasma gondii*. Biocell 25, 53–59.

Méresse S, Steele-Mortimer O, Finlay BB, Gorvel JP (1999). The rab7 GTPase controls the maturation of *Salmonella typhimurium*-containing vacuoles in HeLa cells. EMBO J 18, 4394–4403.

Mordue DG, Desai N, Dustin M, Sibley LD (1999a). Invasion by *Toxoplasma gondii* establishes a moving junction that selectively excludes host cell plasma membrane proteins on the basis of their membrane anchoring. J Exp Med 190, 1783–1792.

Mordue DG, Håkansson S, Niesman I, Sibley LD (1999b). *Toxoplasma gondii* resides in a vacuole that avoids fusion with host cell endocytic and exocytic vesicular trafficking pathways. Exp Parasitol 92, 87–99.

Morisaki JH, Heuser JE, Sibley LD (1995). Invasion of *Toxoplasma gondii* occurs by active penetration of the host cell. J Cell Sci 108 (Pt 6), 2457–2464.

Murata T, Delprato A, Ingmundson A, Toomre DK, Lambright DG, Roy CR (2006). The *Legionella pneumophila* effector protein DrrA is a Rab1 guanine nucleotide-exchange factor. Nat Cell Biol 8, 971–977.

Nam H-W (2009). GRA proteins of *Toxoplasma gondii:* maintenance of host-parasite interactions across the parasitophorous vacuolar membrane. Korean J Parasitol 4 (suppl), S29–S37.

Ng CG, Coppens I, Govindarajan D, Pisciotta J, Shulaev V, Griffin DE (2008). Effect of host cell lipid metabolism on alphavirus replication, virion morphogenesis, and infectivity. Proc Natl Acad Sci USA 105, 16326–16331.

Nichols BA, Chiappino ML, O'Connor GR (1983). Secretion from the rhoptries of *Toxoplasma gondii* during host-cell invasion. J Ultrastruct Res 83, 85–98.

Nozawa K, Casiano CA, Hamel JC, Molinaro C, Fritzler MJ, Chan EKL (2002). Fragmentation of Golgi complex and Golgi autoantigens during apoptosis and necrosis. Arthritis Res 4, R3.

Pagano RE, Martin OC, Kang HC, Haugland RP (1991). A novel fluorescent ceramide analogue for studying membrane traffic in animal cells: accumulation at the Golgi apparatus results in altered spectral properties of the sphingolipid precursor. J Cell Biol 113, 1267–1279.

Pfefferkorn ER, Guyre PM (1984). Inhibition of growth of *Toxoplasma gondii* in cultured fibroblasts by human recombinant gamma interferon. Infect Immun 44, 211–216.

Pratt S, Wansadhipathi-Kannangara NK, Bruce CR, Mina JG, Shams-Eldin H, Casas J, Hanada K, Schwarz RT, Sonda S, Denny PW (2013). Sphingolipid synthesis and scavenging in the intracellular apicomplexan parasite, *Toxoplasma gondii*. Mol Biochem Parasitol 187, 43–51.

Proikas-Cezanne T, Gaugel A, Frickey T, Nordheim A (2006). Rab14 is part of the early endosomal clathrin-coated TGN microdomain. FEBS Lett 580, 5241–5246.

Quittnat F *et al.* (2004). On the biogenesis of lipid bodies in ancient eukaryotes: synthesis of triacylglycerols by a *Toxoplasma* DGAT1-related enzyme. Mol Biochem Parasitol 138, 107–122.

Ricard J, Pelloux H, Pathak S, Pipy B, Ambroise-Thomas P (1996). TNF-alpha enhances *Toxoplasma gondii* cyst formation in human fibroblasts through the sphingomyelinase pathway. Cell Signal 8, 439–442.

Romano JD, Bano N, Coppens I (2008). New host nuclear functions are not required for the modifications of the parasitophorous vacuole of *Toxoplasma*. Cell Microbiol 10, 465–476.

Rome ME, Beck JR, Turetzky JM, Webster P, Bradley PJ (2008). Intervacuolar transport and unique topology of GRA14, a novel dense granule protein in *Toxoplasma gondii*. Infect Immun 76, 4865–4875.

Roos DS, Donald RG, Morrissette NS, Moulton AL (1994). Molecular tools for genetic dissection of the protozoan parasite *Toxoplasma gondii*. Methods Cell Biol 45, 27–63.

Rzomp KA, Scholtes LD, Briggs BJ, Whittaker GR, Scidmore MA (2003). Rab GTPases are recruited to chlamydial inclusions in both a species-dependent and species-independent manner. Infect Immun 71, 5855–5870.

Schwab JC, Beckers CJ, Joiner KA (1994). The parasitophorous vacuole membrane surrounding intracellular *Toxoplasma gondii* functions as a molecular sieve. Proc Natl Acad Sci USA 91, 509–513.

Short B, Haas A, Barr FA (2005). Golgins and GTPases, giving identity and structure to the Golgi apparatus. Biochim Biophys Acta 1744, 383–395.

Sibley LD, Niesman IR, Asai T, Takeuchi T (1994). *Toxoplasma gondii*: secretion of a potent nucleoside triphosphate hydrolase into the parasitophorous vacuole. Exp Parasitol 79, 301–311.

Sibley LD, Niesman IR, Parmley SF, Cesbron-Delauw MF (1995). Regulated secretion of multi-lamellar vesicles leads to formation of a tubulo-vesicular network in host-cell vacuoles occupied by *Toxoplasma gondii*. J Cell Sci 108, 1669–1677.

Sinai AP, Webster P, Joiner KA (1997). Association of host cell endoplasmic reticulum and mitochondria with the *Toxoplasma gondii* parasitophorous vacuole membrane: a high affinity interaction. J Cell Sci 110, 2117–2128.

Sinka R, Gillingham AK, Kondylis V, Munro S (2008). Golgi coiled-coil proteins contain multiple binding sites for Rab family G proteins. J Cell Biol 183, 607–615.

Sonda S, Sala G, Ghidoni R, Hemphill A, Pieters J (2005). Inhibitory effect of aureobasidin A on *Toxoplasma gondii*. Antimicrob Agents Chemother 49, 1794–1801.

Striepen B, Soldati-Favre D (2007). Genetic manipulation of *Toxoplasma gondii*. In: *Toxoplasma Gondii*. The Model Apicomplexan: Perspectives and Methods, ed. LM Weiss and K Kim, London: Elsevier, 391–415.

Suss-Toby E, Zimmerberg J, Ward GE (1996). *Toxoplasma* invasion: the parasitophorous vacuole is formed from host cell plasma membrane and pinches off via a fission pore. Proc Natl Acad Sci USA 93, 8413–8418.

Suzuki Y (2002). Immunopathogenesis of cerebral toxoplasmosis. J Infect Dis 186 (Suppl 2), S234–S240.

Thomas C, Rousset R, Noselli S (2009). JNK signalling influences intracellular trafficking during *Drosophila* morphogenesis through regulation of the novel target gene Rab30. Dev Biol 331, 250–260.

Via LE, Deretic D, Ulmer RJ, Hibler NS, Huber LA, Deretic V (1997). Arrest of mycobacterial phagosome maturation is caused by a block in vesicle fusion between stages controlled by rab5 and rab7. J Biol Chem 272, 13326–13331.

Walker ME, Hjort EE, Smith SS, Tripathi A, Hornick JE, Hinchcliffe EH, Archer W, Hager KM (2008). *Toxoplasma gondii* actively remodels the microtubule network in host cells. Microbes Infect 10, 1440–1449.

Wang Y, Weiss LM, Orlofsky A (2010). Coordinate control of host centrosome position, organelle distribution, and migratory response by *Toxoplasma gondii* via host mTORC2. J Biol Chem 285, 15611–15618.

Wilson BS, Nuoffer C, Meinkoth JL, McCaffery M, Feramisco JR, Balch WE, Farquhar MG (1994). A Rab1 mutant affecting guanine nucleotide exchange promotes disassembly of the Golgi apparatus. J Cell Biol 125, 557–571.

Wu BX, Clarke CJ, Hannun YA (2010). Mammalian neutral sphingomyelinases: regulation and roles in cell signaling responses. Neuromol Med 12, 320–330.

Zhang K, Bangs JD, Beverley SM (2010). Sphingolipids in parasitic protozoa. Adv Exp Med Biol 688, 238–248.